Quantum Classical Correspondence for a non-Hermitian Bose-Hubbard Dimer

Eva-Maria Graefe[1,2], Hans Jürgen Korsch[2], and Astrid Elisa Niederle[2,3]
[1] *School of Mathematics, University of Bristol, Bristol, BS8 1TW, UK*
[2] *FB Physik, TU Kaiserslautern, D–67653 Kaiserslautern, Germany*
[3] *Theoretical Physics, Saarland University, D–66041 Saarbrücken, Germany*
(Dated: December 15, 2014)

We investigate the many-particle and mean-field correspondence for a non-Hermitian N-particle Bose-Hubbard dimer where a complex onsite energy describes an effective decay from one of the modes. Recently a generalized mean-field approximation for this non-Hermitian many-particle system yielding an alternative complex nonlinear Schrödinger equation was introduced. Here we give details of this mean-field approximation and show that the resulting dynamics can be expressed in a generalized canonical form that includes a metric gradient flow. The interplay of nonlinearity and non-Hermiticity introduces a qualitatively new behavior to the mean-field dynamics: The presence of the non-Hermiticity promotes the self-trapping transition, while damping the self-trapping oscillations, and the nonlinearity introduces a strong sensitivity to the initial conditions in the decay of the normalization. Here we present a complete characterization of the mean-field dynamics and the fixed point structure. We also investigate the full many-particle dynamics, which shows a rich variety of breakdown and revival as well as tunneling phenomena on top of the mean-field structure.

PACS numbers: 03.65.-w, 03.75.Kk, 05.30.Jp

I. INTRODUCTION

In the past decade the theoretical investigation of Bose-Einstein condensates led to a widespread interest in nonlinear quantum theories such as the nonlinear Schrödinger equation of Gross-Pitaevskii type [1]. In contrast to nonlinear generalizations of quantum mechanics at a fundamental level [2], in the context of ultracold atoms the nonlinearity arises as the consequence of an effective single particle description in a mean-field approximation of an initially linear many-particle quantum system. This limit is formally similar to the classical limit of standard single particle quantum mechanics. In this spirit the mean-field approximation is often formulated as a replacement of the particle creation and annihilation operators with c-numbers that describe the amplitudes of the effective single particle wave function. The time evolution is then governed by canonical equations of motion based on the fact that nonlinear as well as linear quantum dynamics can be formulated as special cases of classical canonical dynamics on the phase space of pure states, the projective Hilbert space. Thus, for Hermitian systems, the correspondence between the many-particle description and the mean-field approximation can be investigated in analogy with the usual quantum classical correspondence for a single particle system [3–8]. In particular the Bose-Hubbard dimer that models N bosons in only two modes, became a standard example many of whose features can be analytically understood [9–16].

For both many-particle and single-particle quantum mechanics, the Hamiltonian is usually demanded to be Hermitian for the description of closed systems. However, there is a rapidly growing interest in the use of non-Hermitian Hamiltonians arising from different areas. The first is the field of open quantum systems where complex energies with negative imaginary parts are used to describe an overall probability decrease that models decay, transport or scattering phenomena (see, e.g., [17–22] and references therein). Although in most cases these non-Hermitian Hamiltonians are introduced heuristically, they can be derived in a mathematically satisfactory way starting from a system coupled to a continuum of states (see, e.g., [19, 23] and references cited therein). It is interesting to note that within the past decade a somewhat orthogonal motivation also generated considerable interest in the physics of non-Hermitian operators. This is based on the observation that a class of non-Hermitian Hamiltonians respecting a certain antilinear symmetry, often referred to as $\mathcal{PT}$-symmetry, yields purely real eigenvalues in some parameter regions [24]. Further, with the introduction of an appropriate inner product they can be used to define a fully consistent quantum theory for closed systems [25]. The so-called $\mathcal{PT}$-symmetric Hamiltonians have been the subject of extensive studies in the past decade see, e.g. [26]. Recently there is increasing interest in $\mathcal{PT}$-symmetric systems in the context of optics [27–33], where first experimental results could be obtained [34, 35]. Non-Hermitian quantum dynamics differ drastically from their unitary counterparts, and their generic features are far from being fully understood. In particular, the investigation of the quantum classical correspondence for non-Hermitian systems is only at its beginning [22, 36–40].

Recently, considerable attention has been paid to non-Hermitian extensions of the Gross-Pitaevskii equation including an imaginary potential, in the context of scattering and transport behavior of BECs [41–46], as well as the implications of decay or leaking boundary conditions in partially open traps [47–50]. The corresponding non-Hermitian nonlinear Schrödinger equations have been formulated in an *ad hoc* manner as a complex generalization of the mean-field description in the Hermitian case. However, for a many-particle system the generalization of the mean-field approximation in the presence of a complex potential is nontrivial and intimately related to the semiclassical limit of non-Hermitian single particle quantum theories. Recently, a derivation starting from a non-Hermitian many-particle system has been presented in [51] for an open Bose-Hubbard dimer [52, 53] described by

the Hamiltonian

$$\hat{\mathcal{H}} = \varepsilon(\hat{a}_1^\dagger\hat{a}_1 - \hat{a}_2^\dagger\hat{a}_2) - 2i\gamma\hat{a}_1^\dagger\hat{a}_1 + v(\hat{a}_1^\dagger\hat{a}_2 + \hat{a}_1\hat{a}_2^\dagger) + \frac{c}{2}(\hat{a}_1^\dagger\hat{a}_1 - \hat{a}_2^\dagger\hat{a}_2)^2. \quad (1)$$

Here $\hat{a}_j$ and $\hat{a}_j^\dagger$ are bosonic annihilation and creation operators for mode j, v is the coupling constant, and c is the strength of the onsite interaction. For convenience we assume both v and c to be positive in the following. The system is opened by making the onsite energy of mode 1 complex. Note that the expectation value of the particle number $\hat{N} = \hat{a}_1^\dagger\hat{a}_1 + \hat{a}_2^\dagger\hat{a}_2$ is conserved and the opening describes a decay of the overall probability encoded in the normalization of the many-particle wave function. A direct experimental realization of the Hamiltonian (1) can be achieved by using ultracold bosonic atoms in a finite double-well trap, confined by a small tunneling barrier on one side and an approximately infinite barrier on the other. The parameter γ can then be tuned in the experiment by lowering or raising the tunnel barrier. An imaginary energy shift $\hat{\mathcal{H}} = \hat{\mathcal{H}}_{\mathcal{PT}} - i\gamma\hat{N}$ transforms this non-Hermitian Bose-Hubbard dimer into a model that is $\mathcal{PT}$-symmetric in the unbiased case ($\varepsilon = 0$):

$$\hat{\mathcal{H}}_{\mathcal{PT}} = (\varepsilon - i\gamma)(\hat{a}_1^\dagger\hat{a}_1 - \hat{a}_2^\dagger\hat{a}_2) + v(\hat{a}_1^\dagger\hat{a}_2 + \hat{a}_2^\dagger\hat{a}_1) + \frac{c}{2}(\hat{a}_1^\dagger\hat{a}_1 - \hat{a}_2^\dagger\hat{a}_2)^2. \quad (2)$$

In the present article we provide a detailed description of the mean-field approximation for this non-Hermitian many-particle system introduced in [51]. Furthermore, we show that the mean-field dynamics can be formulated in terms of generalized canonical evolution equations on the classical phase space given by the Bloch sphere. These equations consist of a combination of a familiar Hamiltonian flow and an additional gradient flow that accounts for damping. This structure was recently introduced as the classical limit of non-Hermitian quantum theories on a flat phase space [22] and it is likely that it holds for arbitrary phase space geometries. It is closely related also to canonical formulations of classical dissipative dynamics that have been investigated in the past two decades [54–58]. The full many-particle dynamics can be understood as quantum behavior on top of the generalized classical structure, incorporating breakdown and revival phenomena as well as tunneling effects.

The article is organized as follows: In section II we provide the background of the non-Hermitian single particle two-level system, and introduce a renormalized Bloch representation for the dynamics. Further, some concepts of non-Hermitian quantum mechanics that are of relevance in the following are provided. In section III the non-Hermitian Bose-Hubbard dimer is introduced as a many-boson generalization of the non-Hermitian two-level system. In section IV we review the generalized mean-field approximation introduced in [51] and show that it can be expressed in a canonical form of dissipative classical mechanics suggested in [22]. We analyze the resulting mean-field dynamics in detail in section V and compare it to the full many-particle system in section VI. We end with a brief summary and an outlook.

II. THE NON-HERMITIAN TWO-LEVEL SYSTEM

The non-Hermitian Bose-Hubbard dimer (1) can be regarded as an N boson generalization of a single particle two-level system with an imaginary energy term modeling a decay from one of the states, which can be described by the 2×2 Hamiltonian

$$\hat{H} = \begin{pmatrix} \varepsilon - 2i\gamma & v \\ v & -\varepsilon \end{pmatrix}, \quad \varepsilon, v, \gamma \in \mathbb{R},\ \gamma > 0. \quad (3)$$

Here the state with the lower onsite energy is assumed to be stable and the other one to decay with a width γ. The general case of two decaying states differs from this model only by an imaginary energy offset. Despite its simplicity the system (3) incorporates many of the generic features of non-Hermitian quantum mechanics and was the subject of many studies in the past (see, e.g., [21, 59–62]). In this section we briefly review some features of this system and a related $\mathcal{PT}$-symmetric model. Furthermore, we present a less familiar representation of the Bloch dynamics.

The non-Hermitian two-level system (3) is intimately related to a prominent $\mathcal{PT}$-symmetric toy-model. Applying a constant energy shift $\hat{H} \to \hat{H} + i\gamma\mathbb{1}$, that is, $\psi \to \psi e^{\gamma t}$, the system (3) can be mapped onto the Hamiltonian

$$\hat{H}_{\mathcal{PT}} = \begin{pmatrix} \varepsilon - i\gamma & v \\ v & -\varepsilon + i\gamma \end{pmatrix}, \quad (4)$$

which is $\mathcal{PT}$-symmetric for $\varepsilon = 0$. Introducing the discrete parity operator

$$\mathcal{P} = \begin{pmatrix} 0 & 1 \\ 1 & 0 \end{pmatrix} \quad (5)$$

that interchanges the two levels and the time reversal operator $\mathcal{T} : i \to -i$ that performs a complex conjugation, we see that $\hat{H}$ commutes with $\mathcal{PT}$, whereas it commutes neither with $\mathcal{P}$ nor with $\mathcal{T}$ alone. Although in the general case for $\varepsilon \neq 0$ the Hamiltonian (4) is not $\mathcal{PT}$-symmetric, to distinguish it from the purely decaying system (3) we shall refer to it as $\mathcal{PT}$-symmetric in the following.

The eigenvalues of the $\mathcal{PT}$-symmetric two-level system are given by

$$\lambda_\pm = \pm\sqrt{(\varepsilon - i\gamma)^2 + v^2} = E_\pm - i\Gamma_\pm. \quad (6)$$

Thus, although the Hamiltonian is not Hermitian, for certain parameters it has a purely real spectrum. In fact in the unbiased case $\varepsilon = 0$ there is a whole region in parameter space $|\gamma| \leq |v|$ in which the spectrum is real. This is illustrated in Fig. 1, which shows the eigenvalues of $\hat{H}_{\mathcal{PT}}$ as a function of γ for $\varepsilon = 0$ and $v = 1$. In the regions of purely real eigenvalues all eigenvectors are simultaneous eigenvectors of the $\mathcal{PT}$-operator; this is often denoted as unbroken $\mathcal{PT}$-symmetry. The eigenvalues of the decaying system (3) are always complex with a negative imaginary part, which is degenerate for both eigenvalues in the regions were the $\mathcal{PT}$-symmetric system has a purely real spectrum.

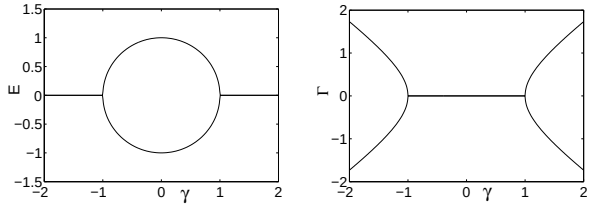

FIG. 1: Real (left) and imaginary (right) parts of the eigenvalues (6) of the $\mathcal{PT}$-symmetric two level system in dependence on the parameter γ for $v = 1$.

The eigenvalues of both the $\mathcal{PT}$-symmetric and the decaying systems degenerate along lines in the parameter space which are specified by

$$\varepsilon = 0 \quad \text{and} \quad v = \pm\gamma. \tag{7}$$

For $\gamma = 0$ this reduces to the so-called diabolical point of the Hermitian two level system [63]. At the complex degeneracies for $\gamma \neq 0$, the exceptional points (EP) [21, 53, 60, 64], the essence of the peculiar behavior of non-Hermitian systems becomes apparent. At an EP not only the eigenvalues, but also the eigenvectors coincide. Thus, while the eigenvectors build a basis of the Hilbert space outside the EP when they coincide at the EP they are not sufficient to span the Hilbert space. In other words, along the exceptional lines (7) the Hamiltonian is not diagonalizable but equivalent to a Jordan block. The occurrence of EPs can have crucial impact on the physical behavior of a system (see, e.g., [21, 28, 29, 65–67]). For the $\mathcal{PT}$-symmetric system (4) the EPs mark the border to the region of broken $\mathcal{PT}$-symmetry where the eigenvalues are complex [53].

In the region of unbroken $\mathcal{PT}$-symmetry the system (4) shows a pseudo-closed behavior. This means that with the introduction of an appropriate inner product the time evolution can be expressed in a unitary way. However, this should not be confused with the conservation of the usual probability as it is given by the normalization of the wave function in the original inner product space $||\psi||^2$. While this is conserved for the time evolution in an eigenstate with real energy, this is in general not true for an arbitrary initial state, due to the nonorthogonality of the eigenfunctions.

The dynamics of a two-level quantum system can easily be expressed in closed form. For a time independent Hamiltonian $\hat{H}$ the Schrödinger equation $i\dot{\psi} = \hat{H}\psi$ with the initial condition $\psi(t=0) = \psi_0$ is solved by $\psi(t) = \hat{U}(t)\psi_0$, where $\hat{U}(t) = \exp(-i\hat{H}t)$ is the time evolution operator. For the $\mathcal{PT}$-symmetric two-level system (4) outside the EP one finds:

$$\hat{U}(t) = \begin{pmatrix} \cos(\omega t) - i\zeta\frac{\sin(\omega t)}{\omega} & -iv\frac{\sin(\omega t)}{\omega} \\ -iv\frac{\sin(\omega t)}{\omega} & \cos(\omega t) + i\zeta\frac{\sin(\omega t)}{\omega} \end{pmatrix}, \tag{8}$$

with the complex energy $\zeta = \varepsilon - i\gamma$, and accordingly the complex frequency $\omega = \sqrt{\zeta^2 + v^2}$, which is determined by the eigenvalue difference $\omega = \frac{1}{2}(\lambda_+ - \lambda_-)$. However, at the EP ($\zeta = -iv$) the frequency goes to zero. In this limit the time evolution operator is given by

$$\hat{U}_{\rm EP}(t) = \begin{pmatrix} 1 - vt & -ivt \\ -ivt & 1 + vt \end{pmatrix}. \tag{9}$$

The time evolution of the normalization $n = |\psi_1|^2 + |\psi_2|^2$ is determined by the population imbalance according to the relation

$$\dot{n} = -2\gamma(|\psi_1|^2 - |\psi_2|^2). \tag{10}$$

From the behavior of the $\mathcal{PT}$-symmetric system the dynamics of the non-Hermitian two-level system (3) can be found by applying the time dependent transformation $\psi(t) \to e^{-\gamma t}\psi(t)$.

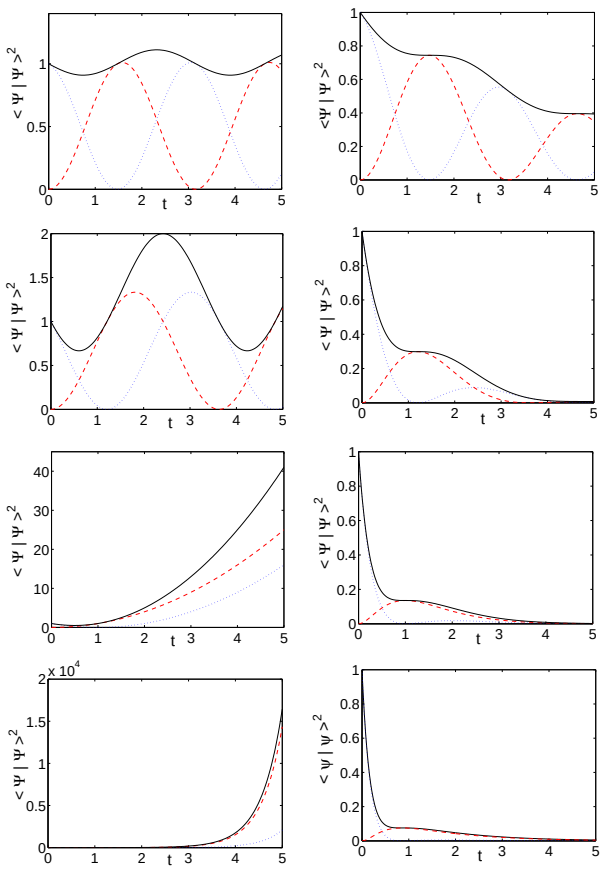

FIG. 2: (Color online) Dynamics of the $\mathcal{PT}$-symmetric (4) (left) and the decaying (3) (right) non-Hermitian two-level system with $\varepsilon = 0$, $v = 1$, and different values of γ (from top to bottom: $\gamma = 0.1, 0.5, 1, 1.5$) for an initial state in level 1. Shown here are the absolute values of the components of the wave function $|\psi_1|^2$ (blue dotted line) and $|\psi_2|^2$ (red dashed line) as well as the total probability $n = |\psi_1|^2 + |\psi_2|^2$ (black solid line).

Figure 2 shows some examples of the dynamics for different non-Hermiticities γ with $\varepsilon = 0$, $v = 1$, and for an initial state in level 1. The left column shows the dynamics for the $\mathcal{PT}$-symmetric system (4) and the right column for the decaying system (3) for the same parameter values. It can be seen that for the $\mathcal{PT}$-symmetric system the normalization oscillates for $\gamma < v$ with a period that increases with increasing

γ and diverges to infinity as γ approaches the EP, $\gamma = v$. The rate of decrease of the normalization takes its maximum value when the population is in the first level; growth and decrease rates are balanced when both levels are equally populated; and the growth rate is maximal when the population in the second level is maximal. We observe that while for small values of γ the system performs Rabi-type oscillations between the two levels, the population oscillations within each level become parallel when the EP is approached. This nicely illustrates the fact that a complex term in the energy cannot be regarded as an overall modulation of the normalization of the system, but rather changes the full dynamics in a dramatic way. The oscillatory behavior breaks down completely at the EP where the period diverges. Instead we observe an algebraic growth of the probability. This can be obtained analytically from $\psi(t) = \hat{U}_{\rm EP}(t)\psi(0)$, with the initial state in level 1, as

$$n(t) = 1 - 2vt + 2v^2t^2. \tag{11}$$

For larger values of γ, the $\mathcal{PT}$-symmetry is broken and so is the balance between growth and decrease – the normalization grows exponentially.

For the purely decaying system (3), on the other hand, we observe a monotonic decrease of the normalization. The decay behavior is not exponential, which is intuitively understood by recalling that the population only decays from one of the levels. Therefore, the decrease is determined by the population of this level, which varies in time if the system is not in an eigenstate. It is interesting to note that in contrast to the $\mathcal{PT}$-symmetric system, we cannot detect an obvious trace of the presence of the EP in the decay dynamics for the non-Hermitian system (3).

The similarity of the optical wave equations in waveguide structures to the Schrödinger equation makes it possible to observe the described dynamics and the $\mathcal{PT}$-related phase transition in optical waveguide structures with gain and loss. This has not only been investigated theoretically [27, 29], but has recently been realized experimentally [34, 35].

Although the non-Hermitian Schrödinger equation does not preserve the normalization, it is possible to describe the dynamics of the system consistently in terms of a Bloch vector that stays confined to the surface of the Bloch sphere throughout the time evolution. For this purpose we first define the renormalized state vector with the components

$$\varphi_j = \frac{\psi_j}{\sqrt{|\psi_1|^2 + |\psi_2|^2}}. \tag{12}$$

For both the decaying (3) and the $\mathcal{PT}$-symmetric system (4) the dynamics are then governed by the non-Hermitian (and nonlinear) effective Schrödinger equation:

$$\mathrm{i}\frac{\mathrm{d}}{\mathrm{d}t}\begin{pmatrix}\varphi_1\\ \varphi_2\end{pmatrix} = \begin{pmatrix}\varepsilon - \mathrm{i}\gamma(1-\kappa) & v\\ v & -\varepsilon + \mathrm{i}\gamma(1+\kappa)\end{pmatrix}\begin{pmatrix}\varphi_1\\ \varphi_2\end{pmatrix}, \tag{13}$$

with $\kappa = |\varphi_1|^2 - |\varphi_2|^2$. This dynamics by definition conserves the normalization $|\varphi_1|^2 + |\varphi_2|^2 = 1$. We can then define the components of the normalized Bloch vector in the familiar way with respect to the renormalized wave function φ:

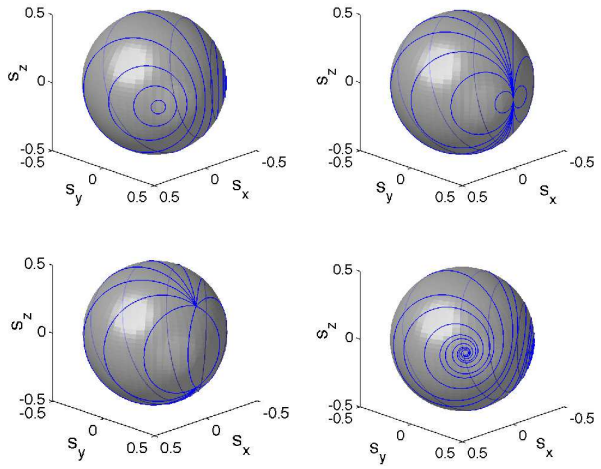

FIG. 3: Effective Bloch dynamics of the non-Hermitian two level system (15) with $v = 1$ and different values of ε and γ. The two plots on the top and the left plot on the bottom are for the unbiased system with $\varepsilon = 0$ and increasing values of $\gamma = 0.75$, 1, 1.25, respectively. The right plot on the bottom shows the dynamics for a biased systems with $\varepsilon = 0.1$ and $\gamma = 0.75$.

$$\begin{aligned} s_x &= \tfrac{1}{2}(\varphi_1^*\varphi_2 + \varphi_1\varphi_2^*) &&= \frac{1}{2}\frac{\psi_1^*\psi_2 + \psi_1\psi_2^*}{\psi_1^*\psi_1 + \psi_2^*\psi_2}\\ s_y &= \tfrac{1}{2\mathrm{i}}(\varphi_1^*\varphi_2 - \varphi_1\varphi_2^*) &&= \frac{1}{2\mathrm{i}}\frac{\psi_1^*\psi_2 - \psi_1\psi_2^*}{\psi_1^*\psi_1 + \psi_2^*\psi_2}\\ s_z &= \tfrac{1}{2}(\varphi_1^*\varphi_1 - \varphi_2^*\varphi_2) &&= \frac{1}{2}\frac{\psi_1^*\psi_1 - \psi_2^*\psi_2}{\psi_1^*\psi_1 + \psi_2^*\psi_2}. \end{aligned} \tag{14}$$

Using this definition we can obtain the generalized Bloch equations of motion from (13) as

$$\begin{aligned} \dot{s}_x &= -2\varepsilon s_y + 4\gamma s_x s_z\\ \dot{s}_y &= 2\varepsilon s_x - 2v s_z + 4\gamma s_y s_z\\ \dot{s}_z &= 2v s_y - \gamma(1 - 4s_z^2). \end{aligned} \tag{15}$$

Here again the normalization $s_x^2 + s_y^2 + s_z^2 = \frac{1}{4}$ is conserved by construction.

The dynamics of the renormalized quantities decouple from the time dependency of the normalization $n = |\psi_1|^2 + |\psi_2|^2$ of the state vector which can be obtained from the Bloch dynamics via

$$\dot{n} = \begin{cases} -4\gamma(s_z + \frac{1}{2})n, & \text{for (3)}\\ -4\gamma s_z n, & \text{for (4).}\end{cases} \tag{16}$$

This allows a separate investigation of both dynamics.

The Bloch dynamics is organized according to the fixed points (the stationary states), which can be obtained analytically from the real roots of the fourth order polynomial

$$16\gamma^2 s_z^4 + 4(\varepsilon^2 + v^2 - \gamma^2)s_z^2 - \varepsilon^2 = 0, \tag{17}$$

where the corresponding s_y and s_x values are given by $s_y = \frac{\gamma}{2v}(1-4s_z^2)$ and the normalization condition. For every parameter set there are only two fixed points which can be of different types, including sinks and sources. In general the type of the fixed points can be identified from the behavior of the surrounding vector field in a systematic manner, which we postpone to the discussion of the general nonlinear case in section V.

In Fig. 3 we show four examples of the Bloch dynamics, three for an unbiased system with $\varepsilon = 0$ and different values of γ, and one where all parameters are nonzero. In the first plot (top on the left) in Fig. 3, where $\gamma < v$, we observe Rabi-type oscillations surrounding one of the two fixed points located at $s_z = 0$. However, compared to the Hermitian case the picture is deformed. The two fixed points are not centered at $s_y = 0$ corresponding to a phase difference of zero and π between the amplitudes in the two levels, respectively, but with increasing γ they approach each other along the equator toward $s_y = \frac{1}{2}$ and $s_x = 0$. This is connected to the fact that the strict $\mathcal{P}$-symmetry which enforces both s_z and s_y to be zero in the Hermitian case, with $\varepsilon, \gamma = 0$, is broken for $\gamma \neq 0$ and first replaced by the $\mathcal{PT}$-symmetry, which only demands that $s_z = 0$. At the EP $\gamma = v$ (shown in the right plot on top in Fig. 3) the two fixed points meet and the symmetry is broken. For even larger values of γ one of the fixed points becomes a sink of the dynamics, and the other a source, both located at $s_z \neq 0$, that is, they belong to configurations where one of the levels is favored despite the symmetry of the system. This could be denoted as a *decay-trapping*. With increasing values of γ the sink approaches the south pole of the Bloch sphere (corresponding to the stable level) and the source approaches the north pole (corresponding to the level from which the decay happens). This is due to the fact that the Bloch dynamics describes the mean values of the remaining part of the population which moves away from the center of the decay. For nonvanishing ε the system is not $\mathcal{PT}$-symmetric, and the situation is changed. In this case the fixed points change into a sink and a source for arbitrary small values of γ. An example of the non-Hermitian Bloch dynamics for $\varepsilon \neq 0$ is depicted in the lower right plot in Fig. 3.

III. THE NON-HERMITIAN BOSE-HUBBARD MODEL

The non-Hermitian Bose-Hubbard dimer (1) can now be defined as the single particle non-Hermitian two-level system (3) populated with N bosons, with the bosonic particle creation and annihilation operators $\hat{a}_j^\dagger$, $\hat{a}_j$ for the two levels that fulfill the usual bosonic commutation relations $[\hat{a}_j, \hat{a}_k^\dagger] = \delta_{jk}$, $[\hat{a}_1, \hat{a}_2] = 0$.

A non-Hermitian many-particle Hamiltonian of the present type does not describe the loss of individual particles. Rather, it describes the decrease in time of the probability to find the entire many-particle ensemble in the two modes. This information is completely encoded in the normalization of the many-particle wave function $|\Psi\rangle$. The expectation value of the particle number operator $\langle\Psi|\hat{N}|\Psi\rangle / \langle\Psi|\Psi\rangle$ stays constant in time. In other words, the "decay" is regarded as a feature of the state, rather than of the particles. The fact that the Hamiltonian (1) commutes with the number operator $\hat{N}$ implies that the matrix representation in the Fock (particle number) basis has a block diagonal structure, that is, it does not induce coupling between subspaces associated with different particle numbers. Therefore, in what follows we shall restrict our discussion to these subspaces of fixed N.

In analogy with the Bloch representation of the single particle system, the Hamiltonian (1) can also be expressed in the form of an angular momentum system. Introducing the angular momentum operators $\hat{L}_x$, $\hat{L}_y$ and $\hat{L}_z$ according to the Schwinger representation

$$\hat{L}_x = \tfrac{1}{2}(\hat{a}_1^\dagger \hat{a}_2 + \hat{a}_1 \hat{a}_2^\dagger), \qquad \hat{L}_y = \tfrac{1}{2\mathrm{i}}(\hat{a}_1^\dagger \hat{a}_2 - \hat{a}_1 \hat{a}_2^\dagger), \\ \hat{L}_z = \tfrac{1}{2}(\hat{a}_1^\dagger \hat{a}_1 - \hat{a}_2^\dagger \hat{a}_2), \tag{18}$$

which obey the usual $SU(2)$ commutation relation

$$[\hat{L}_x, \hat{L}_y] = \mathrm{i}\hat{L}_z, \tag{19}$$

and its cyclic permutations, the Hamiltonian (1) can be reformulated in the form

$$\hat{\mathcal{H}} = 2(\varepsilon - \mathrm{i}\gamma)\hat{L}_z + 2v\hat{L}_x + 2c\hat{L}_z^2 - \mathrm{i}\gamma\hat{N}. \tag{20}$$

The conservation of $\hat{N}$ appears as the conservation of $\hat{L}^2 = \frac{\hat{N}}{2}\left(\frac{\hat{N}}{2}+1\right)$, i.e. the rotational quantum number $l = N/2$.

In the standard basis of the angular momentum algebra $|l,m\rangle$, which can be defined by the relations

$$\begin{aligned} \hat{L}_\pm |l,m\rangle &= \sqrt{(l \mp m)(l \pm m + 1)}\,|l, m \pm 1\rangle, \\ \hat{L}_z |l,m\rangle &= m|l,m\rangle \end{aligned} \tag{21}$$

with $l = N/2$, the Hamiltonian $\hat{\mathcal{H}}$ takes the form of a tridiagonal $(N+1)\times(N+1)$-matrix. Special features of the spectrum of the present model and a corresponding $\mathcal{PT}$-symmetric model are discussed in [52, 53].

In the limit of vanishing particle interaction, $c = 0$, the eigenvalue equation is solvable in closed form and the spectrum consists of multiples of the single particle eigenvalues:

$$\lambda_n = -\mathrm{i}N\gamma + (2n - N)\sqrt{(\varepsilon - \mathrm{i}\gamma)^2 + v^2}, \quad n = 0, 1, ..., N. \tag{22}$$

Thus, for $\varepsilon = 0$ at $\gamma = \pm v$ all eigenvalues degenerate simultaneously. The corresponding eigenvectors also coalesce and this configuration thus corresponds to a full Jordan block structure of the Hamiltonian, that is, an EP of higher order [53]. As for the single particle system the unbiased ($\varepsilon = 0$) non-Hermitian Bose-Hubbard dimer can be mapped into a $\mathcal{PT}$-symmetric model (2) by an imaginary energy shift $\hat{\mathcal{H}} = \hat{\mathcal{H}}_{\mathcal{PT}} - \mathrm{i}\gamma\hat{N}$. For this model the $\mathcal{PT}$-symmetry is broken at the EP where all eigenvalues become complex simultaneously. An arbitrary small interaction strength $c \neq 0$ perturbs the system in a manner that leads to a splitting of the EP of higher order into a series of EPs of second order, that is, degeneracies of pairs of eigenvalues and the corresponding eigenvectors. The interaction thereby always shrinks the region of unbroken

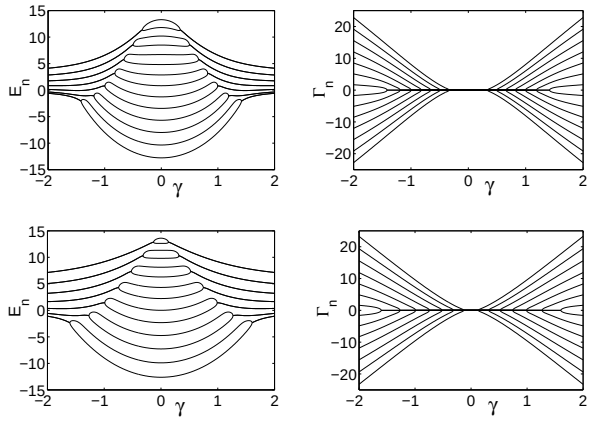

FIG. 4: Real (left) and imaginary (right) parts of the eigenvalues $\lambda_n = E_n - \mathrm{i}\Gamma_n$ of the Bose-Hubbard Hamiltonian (2) as a function of the non-Hermiticity γ for $v = 1$, $N = 13$ particles and $c = 0.5/N$ (top) and $c = 0.9/N$ (bottom).

$\mathcal{PT}$-symmetry. In Fig. 4 we show the eigenvalues for $N = 13$ particles in dependence on the non-Hermiticity γ for two values of the interaction strength. It can be seen that the region of purely real eigenvalues shrinks with increasing interaction strength. Further details concerning the spectral behavior of the $\mathcal{PT}$-symmetric model (2) can be found in [53]. Some general aspects of $\mathcal{PT}$-symmetric models of Lie-algebraic type as the present one have been presented in [68].

The many-particle dynamics can be conveniently analyzed in terms of the angular momentum expectation values. The non-Hermitian generalization of the Heisenberg equation of motion for an operator $\hat{A}$ (which is not explicitly time dependent) is given by [18, 22, 51]

$$\begin{aligned} \mathrm{i}\hbar\frac{\mathrm{d}}{\mathrm{d}t}\langle\psi|\hat{A}|\psi\rangle &= \langle\psi|\hat{A}\hat{\mathcal{H}} - \hat{\mathcal{H}}^{\dagger}\hat{A}|\psi\rangle \\ &= \langle\psi|\,[\hat{A},\hat{H}]|\psi\rangle - i\langle\psi|\,[\hat{A},\hat{\Gamma}]_{+}|\psi\rangle, \end{aligned} \quad (23)$$

where we decomposed the Hamiltonian into Hermitian and anti-Hermitian parts via $\hat{\mathcal{H}} = \hat{H} - \mathrm{i}\hat{\Gamma}$, with $\hat{H} = \hat{H}^{\dagger}$ and $\hat{\Gamma} = \hat{\Gamma}^{\dagger}$, and introduced the notation $[\,,\,]_{+}$ for the anti-commutator. Thus, the equation of motion for the expectation value $\langle\hat{A}\rangle = \langle\psi|\hat{A}|\psi\rangle/\langle\psi|\psi\rangle$ reads [22, 51]

$$\mathrm{i}\hbar\frac{\mathrm{d}}{\mathrm{d}t}\langle\hat{A}\rangle = \langle[\hat{A},\hat{H}]\rangle - 2\mathrm{i}\,\Delta^2_{A\Gamma}, \quad (24)$$

with the covariance $\Delta^2_{A\Gamma} = \langle\frac{1}{2}[\hat{A},\hat{\Gamma}]_{+}\rangle - \langle\hat{A}\rangle\langle\hat{\Gamma}\rangle$. In the case of the Bose-Hubbard dimer (1), we find for the dynamics of the angular momentum expectation values:

$$\begin{aligned} \tfrac{\mathrm{d}}{\mathrm{d}t}\langle\hat{L}_x\rangle &= -2\varepsilon\langle\hat{L}_y\rangle - 2c\langle[\hat{L}_y,\hat{L}_z]_{+}\rangle - 2\gamma\{2\Delta^2_{\hat{L}_x\hat{L}_z} + \Delta^2_{\hat{L}_x\hat{N}}\} \\ \tfrac{\mathrm{d}}{\mathrm{d}t}\langle\hat{L}_y\rangle &= 2\varepsilon\langle\hat{L}_x\rangle + 2c\langle[\hat{L}_x,\hat{L}_z]_{+}\rangle - 2v\langle\hat{L}_z\rangle - 2\gamma\{2\Delta^2_{\hat{L}_y\hat{L}_z} + \Delta^2_{\hat{L}_y\hat{N}}\} \\ \tfrac{\mathrm{d}}{\mathrm{d}t}\langle\hat{L}_z\rangle &= 2v\langle\hat{L}_y\rangle - 2\gamma\{2\Delta^2_{\hat{L}_z\hat{L}_z} + \Delta^2_{\hat{L}_z\hat{N}}\}, \end{aligned} \quad (25)$$

and the normalization of the many-particle wave function $|\Psi\rangle$ decays according to

$$\frac{\mathrm{d}}{\mathrm{d}t}\langle\Psi|\Psi\rangle = -2\gamma\big\{2\langle\hat{L}_z\rangle + \langle\hat{N}\rangle\big\}\langle\Psi|\Psi\rangle. \quad (26)$$

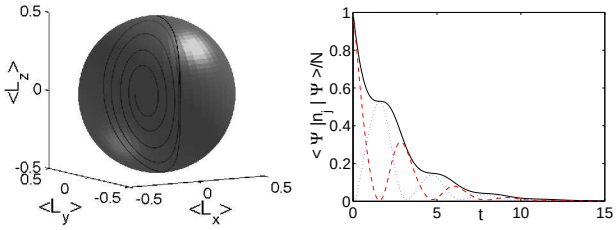

FIG. 5: (Color online) The left plot shows the dynamics of the expectation values of the angular momentum operator for an initial coherent state located at the north pole of the Bloch sphere (the decaying level) for $N = 20$ particles, $v = 1$, $\gamma = 0.01$ and $g = 0.5$. The right plot shows the corresponding decay of the survival probability (full black curve) and the populations of site 1 (dashed red curve) and site 2 (dotted blue curve)

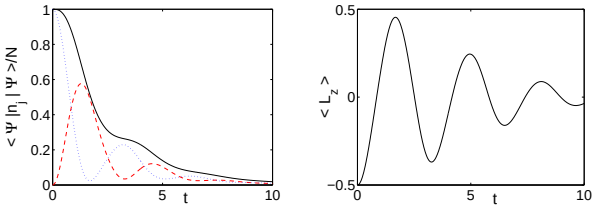

FIG. 6: (Color online) The left plot shows the decay of the survival probability (full black curve) and the populations of site 1 (dashed red curve) and site 2 (dotted blue curve) for an initial coherent state located at the south pole of the Bloch sphere for $N = 20$ particles, $v = 1$, $\gamma = 0.01$ and $g = 1$. The right plot shows the corresponding expectation value of $\hat{L}_z$.

The many-particle angular momentum dynamics becomes identical to the effective Bloch-equations for vanishing interaction, $c = 0$, if the initial state is coherent, as will become clear later. However, to account for the particle number the normalization of the many-particle wave function has to be associated with the N-th power of the single particle wave function.

To get an impression of the behavior for nonvanishing interaction strengths we show an example of the many-particle dynamics for a small value of γ and an intermediate value of the interaction strength c in Fig. 5 for an initial state where all particles are in the decaying mode, that is, a state located at the north pole of the Bloch sphere. The left plot in the figure shows the time evolution of the angular momentum expectation value and the corresponding Bloch sphere. Similarly to the Hermitian case [9, 69] the Bloch vector penetrates the Bloch sphere throughout the time evolution. The right side of the figure shows the decay behavior captured by the normalization of the many-particle wave function and the population probability $\langle\Psi|\hat{n}_j|\Psi\rangle/N$ of the two levels. The momentary decay rate is proportional to the expectation value of the z-component of the angular momentum, that is, the population imbalance of the two-modes. Thus, in comparison with the noninteracting case (that is equivalent to the behavior of the

single particle system investigated in the previous section) the staircase behavior of the decay is slightly changed: The steps are not completely flat, having a negative slope for all times, because the $\hat{L}_z$ component does not reach the stable south pole in the depicted time interval. This behavior becomes more pronounced for stronger interaction strengths, as depicted for an example in Fig. 6 where on the right side the $\hat{L}_z$ expectation value is shown for comparison. The breakdown behavior in the dynamics of the full many-particle observables can be understood as a many particle effect on top of the mean-field dynamics which stays confined to the Bloch sphere and which we shall introduce in the following.

IV. THE GENERALIZED MEAN-FIELD APPROXIMATION AND A CANONICAL STRUCTURE

The mean-field approximation in the Hermitian case is often formulated in close analogy with the classical approximation of single particle quantum mechanics. That is, operators are replaced by c-numbers and commutators by Poisson brackets, and thus, the Heisenberg equations are replaced by Hamiltonian equations. However, this analogy was hitherto of little use for non-Hermitian many-particle systems, as the classical limit of non-Hermitian quantum dynamics itself is still far from being understood. Thus, one had to resort to alternative formulations of the mean-field approximation. For Hermitian quantum systems the classical analog can be derived in an elegant way using coherent states [70, 71]. This method has also proven useful in the investigation of the quantum-classical correspondence for cold atoms in optical lattices described by Bose-Hubbard type Hamiltonians where the condensed states are equivalent to $SU(M)$ coherent states [3, 6, 72]. In [51] a mean-field approximation using generalized coherent states was introduced for the non-Hermitian Bose-Hubbard dimer (1). Here we provide details of this generalized mean-field approximation and connect it to a recently proposed classical approximation for non-Hermitian single particle quantum dynamics [22] where a generalized canonical structure arises. Although it has only been derived for a flat phase space, it has been shown that the mean-field approximation for the present model can be formulated in terms of the proposed generalized canonical equations of motion. From a practical perspective, making use of the generalized canonical structure strongly simplifies the calculation yielding the mean-field dynamics. This is promising for the generalization to larger systems involving more than two states.

The underlying idea of the generalized mean-field approximation [51] is to describe the whole ensemble of many-particles by only one macroscopic wave function in the limit of infinite particle number. In other words, we assume that the particles form a condensate throughout the time evolution. For a two-mode system the fully condensed states can be expressed in the form

$$|x\rangle = \frac{1}{\sqrt{N!}}\left(x_1\hat{a}_1^\dagger + x_2\hat{a}_2^\dagger\right)^N |0,0\rangle, \tag{27}$$

with two complex coefficients that are not necessarily normalized to unity, $n = |x_1|^2 + |x_2|^2$. The condensed many-particle wave function (27) is then normalized to $\langle x|x\rangle = (|x_1|^2+|x_2|^2)^N = n^N$. These states are in fact equivalent to the generalized $SU(2)$ coherent states [71, 73], often denoted also as atomic coherent states. They can be constructed by an arbitrary $SU(2)$ rotation $\hat{R}(\theta,\phi) = \mathrm{e}^{\mathrm{i}\theta(\hat{L}_x\sin\phi - \hat{L}_y\cos\phi)}$ of an extremal Fock state ,e.g., $|N\rangle$, where all particles are in the first mode:

$$|\theta,\phi\rangle = \hat{R}(\theta,\phi)|N\rangle. \tag{28}$$

This is equivalent to (27) if we set

$$x_1 = \sqrt{n}\mathrm{e}^{-\mathrm{i}\phi}\cos\tfrac{\theta}{2}, \quad x_2 = \sqrt{n}\sin\tfrac{\theta}{2}. \tag{29}$$

Thus, the mean-field approximation is equivalent to the assumption that the many-particle state, initially chosen as a coherent state, remains coherent for all times of interest. This assumption is in fact exact if the Hamiltonian is a linear superposition of the generators of the dynamical symmetry group [71], in our case for vanishing interaction $c = 0$. This can be seen by calculating the action of the time evolution operator on an initially coherent state. For nonvanishing interaction it is in general an approximation yielding the mean-field dynamics. The mean-field equations of motion can thus be obtained from the quantum dynamics by replacing all expectation values with their values in coherent states and identifying these with the mean-field quantities. The resulting mean-field dynamics can be interpreted as a special case of constrained quantum motion [74] where the constraint is that the many-particle state is coherent.

Let us now derive the mean-field Bloch dynamics from the equations of motion for the many-particle angular momentum expectation values (25) using the $SU(2)$ coherent state approximation. The expectation values of the $\hat{L}_i$, $i = x,y,z$ in terms of the coherent state coordinates x_1 and x_2 read:

$$\begin{aligned}
\frac{\langle x|\hat{L}_x|x\rangle}{\langle x|x\rangle} &= \frac{N}{2}\frac{x_1^*x_2 + x_1x_2^*}{x_1^*x_1 + x_2^*x_2},\\
\frac{\langle x|\hat{L}_y|x\rangle}{\langle x|x\rangle} &= \frac{N}{2\mathrm{i}}\frac{x_1^*x_2 - x_1x_2^*}{x_1^*x_1 + x_2^*x_2},\\
\frac{\langle x|\hat{L}_z|x\rangle}{\langle x|x\rangle} &= \frac{N}{2}\frac{x_1^*x_1 - x_2^*x_2}{x_1^*x_1 + x_2^*x_2}.
\end{aligned} \tag{30}$$

We can identify these quantities with the components of the corresponding renormalized mean-field Bloch vector:

$$s_j = \langle\hat{L}_j\rangle/N. \tag{31}$$

Comparison with the definition of the mean-field Bloch vector in the single particle case (14) reveals that the coordinates of the coherent state can naturally be associated with the components of the effective single particle wave function ψ. To perform the mean-field approximation we further need the expectation values of the anti-commutators appearing in (25) for $SU(2)$ coherent states which factorize as

$$\begin{aligned}
\langle[\hat{L}_i,\hat{L}_j]_+\rangle &= 2(1-\tfrac{1}{N})\langle\hat{L}_i\rangle\langle\hat{L}_j\rangle + \delta_{ij}\frac{N}{2},\\
\langle[\hat{L}_i,\hat{N}]_+\rangle &= 2N\langle\hat{L}_i\rangle,
\end{aligned} \tag{32}$$

with $N = \langle \hat{N} \rangle$. Inserting these expressions into (25) and taking the macroscopic limit $N \to \infty$ with $Nc = g$ fixed we obtain the desired non-Hermitian mean-field evolution equations:

$$\begin{array}{lllll} \dot{s}_x = & -2\varepsilon s_y & -4g s_y s_z & & +4\gamma s_x s_z, \\ \dot{s}_y = & +2\varepsilon s_x & +4g s_x s_z & -2v s_z & +4\gamma s_y s_z, \\ \dot{s}_z = & & & +2v s_y & -\gamma(1-4s_z^2). \end{array} \tag{33}$$

These nonlinear non-Hermitian Bloch equations are real valued and conserve $s^2 = s_x^2 + s_y^2 + s_z^2 = 1/4$, i.e. the dynamics are regular and confined to the Bloch sphere. The total probability n decays as

$$\dot{n} = -2\gamma(2s_z + 1)\, n. \tag{34}$$

In the limit $g = 0$ in which the assumption that the many-particle state stays coherent in time is exactly fulfilled, these equations reduce to the equations for the linear single particle two level system (15). Thus, as mentioned before, this captures the exact many-particle dynamics in this limit. Generalized Bloch equations related to (33) also appear in a different context, where the influence of decoherence is investigated [75–79]. It should further be noted that they can be considered a special case of the celebrated Landau-Lifshitz equations with Gilbert damping appearing frequently in magnetization dynamics.

Let us now express the mean-field dynamics in the form of a generalized nonlinear Schrödinger equation. In terms of the components ψ_j of the unnormalized wave function (associated with the coordinates x_j of the many-particle coherent state) this can be formulated as:

$$\mathrm{i}\frac{\mathrm{d}}{\mathrm{d}t}\begin{pmatrix}\psi_1\\ \psi_2\end{pmatrix} = \begin{pmatrix}\varepsilon + g\kappa - 2\mathrm{i}\gamma & v \\ v & -\varepsilon - g\kappa\end{pmatrix}\begin{pmatrix}\psi_1\\ \psi_2\end{pmatrix}, \tag{35}$$

with

$$\kappa = \frac{|\psi_1|^2 - |\psi_2|^2}{|\psi_1|^2 + |\psi_2|^2}. \tag{36}$$

The equation of motion for the normalization in this formulation is given by $\dot{n} = -2\gamma(1-\kappa)n$. While in the limit $\gamma \to 0$ the wave function stays normalized and the equations are thus equivalent to the usual discrete nonlinear Schrödinger equation of Gross-Pitaevskii type, the nonlinear term gets modified due to the non-Hermiticity. Alternatively we can express the dynamics in terms of the renormalized wave function $\varphi_j = \psi_j/\sqrt{n}$:

$$\mathrm{i}\frac{\mathrm{d}}{\mathrm{d}t}\begin{pmatrix}\varphi_1\\ \varphi_2\end{pmatrix} = \begin{pmatrix}\varepsilon + g\kappa - \mathrm{i}\gamma(1-\kappa) & v \\ v & -\varepsilon - g\kappa + \mathrm{i}\gamma(1+\kappa)\end{pmatrix}\begin{pmatrix}\varphi_1\\ \varphi_2\end{pmatrix}, \tag{37}$$

with $\kappa = |\varphi_1|^2 - |\varphi_2|^2$. This dynamics by definition conserves the normalization $||\varphi||^2 = 1$.

Note that the dynamics induced by the nonlinear non-Hermitian Schrödinger equation (35) differs fundamentally from the dynamics of a discrete Gross-Pitaevskii equation with an additional imaginary on-site energy, where the nonlinearity is determined by $\kappa = |\psi_1|^2 - |\psi_2|^2$. This latter type of non-Hermitian nonlinear Schrödinger equations has attracted considerable attention in the context of the description of scattering phenomena and the influence of leaking boundaries for Bose-Einstein condensates recently [47–49, 52, 80, 81]. Furthermore, these *ad hoc* nonlinear non-Hermitian equations also appear for absorbing nonlinear waveguides [27–29, 82].

In [22] it has been shown that the mean-field approximation of the non-Hermitian Bose-Hubbard dimer can also be expressed in terms of a generalized canonical structure, as we will review in what follows. The generalized canonical equations of motion proposed in [22] are of the form

$$\begin{pmatrix}\dot{q}\\ \dot{p}\end{pmatrix} = \Omega^{-1}\vec{\nabla}H - G^{-1}\vec{\nabla}\Gamma, \tag{38}$$

where p and q are canonical phase space variables and $\vec{\nabla}$ denotes the phase space gradient, Ω is the symplectic matrix

$$\Omega = \begin{pmatrix}0 & -1\\ 1 & 0\end{pmatrix} \tag{39}$$

and G is the corresponding Kähler metric [83, 84] on the relevant phase space. The classical Hamiltonian function $\mathcal{H} = H - \mathrm{i}\Gamma$ is given by the expectation value of the quantum Hamiltonian in the relevant coherent states. The dynamics of the normalization of the original wave function $n = |\psi_1|^2 + |\psi_2|^2$ is governed by the equation of motion

$$\dot{n} = -2\Gamma n. \tag{40}$$

The dynamical equation (38) is a combination of a canonical symplectic flow generated by the real part H of the Hamiltonian function and a canonical gradient flow generated by the imaginary part Γ. The symplectic part evidently gives rise to the familiar Hamiltonian dynamics of classical mechanics. The gradient vector with a negative sign points in the direction of the steepest descent of the function Γ. Thus, this part of the dynamics aims to drive the system toward the minimum of Γ and can naturally be associated with a damping.

The generalized canonical structure can be used to directly calculate the mean-field dynamics without evaluating the generalized Heisenberg equations of motion and performing the coherent state approximation as follows: Our classical phase space is given by the Bloch sphere and can be parametrized by the canonical variables p and q that are related to the classical Bloch vector via

$$\begin{aligned} s_x &= \tfrac{1}{2}\sqrt{1-p^2}\cos(2q) \\ s_y &= \tfrac{1}{2}\sqrt{1-p^2}\sin(2q) \\ s_z &= \tfrac{1}{2}p. \end{aligned} \tag{41}$$

We can express the expectation value of the many-particle Hamiltonian (1) in $SU(2)$ coherent states in the variables p, q to find the classical Hamiltonian function:

$$H = \varepsilon p + v\sqrt{1-p^2}\cos(2q) + \frac{g}{2}p^2 \quad \text{and} \quad \Gamma = \gamma p. \tag{42}$$

The Kähler metric on the Bloch sphere in the variables q, p is given by [22]

$$G = \begin{pmatrix}2(1-p^2) & 0\\ 0 & \frac{1}{2(1-p^2)}\end{pmatrix}. \tag{43}$$

Evaluating the generalized canonical equations (38) of motion yields

$$\dot{q} = \varepsilon + gp - v\frac{p}{\sqrt{1-p^2}}\cos(2q) \quad (44)$$

$$\dot{p} = -2\gamma(1-p^2) + 2v\sqrt{1-p^2}\sin(2q), \quad (45)$$

which is equivalent to the nonlinear Bloch equations (33). Similar equations also appear in a related model where a different mean-field approximation is applied [85].

We note here that the expressions arising for the $\mathcal{PT}$-symmetric version of the Hamiltonian (4) differ from the present ones by a complex energy shift. Thus, since the generalized canonical equations of motion are invariant under a constant energy shift (as are the usual canonical equations of motion of Hamilton type), the effective dynamics resulting from the Hamiltonian functions related to (3) and (4), respectively, are identical, in agreement with the previous observations.

Note also that the nonlinear Schrödinger equation (37) can be directly formulated as generalized complex canonical equations of motion for the coordinates $\varphi_1, \varphi_1^*, \varphi_2, \varphi_2^*$. However, here one has to take care of the constraints confining the dynamics to the Bloch sphere explicitly and the expression for the metric gets more elaborate (see Appendix A). Thus, for practical purposes the formulation in real canonical variables p, q is more convenient.

V. MEAN-FIELD DYNAMICS AND FIXED POINT STRUCTURE

In this section we analyze the mean-field behavior arising from the interplay of non-Hermiticity and nonlinearity. The mean-field dynamics is organized according to fixed points, which correspond to stationary solutions of the nonlinear complex Schrödinger equation (35). In contrast to the widely investigated behavior of vector fields in $\mathbb{R}^2$, the general features of vector fields on the sphere have rarely been investigated in detail. Only recently some interest in polynomial vector fields as the present one on the two-sphere $\mathbb{S}^2$ has emerged in the mathematical literature [86–89]. In this context it was shown that the upper bound of the number of fixed points for a general polynomial vector field of degree 2 on the sphere is equal to 6.

In the present case there are at most four fixed points that can be obtained analytically as the roots of a fourth order polynomial similar to the Hermitian case [90]. To see this we have to study the fixed point equation defined by (33) with $\vec{s} = 0$, which provides

$$v s_y = 2\gamma\left(\tfrac{1}{4} - s_z^2\right). \quad (46)$$

Using this and the normalization condition $s_x^2 + s_y^2 + s_z^2 = \frac{1}{4}$ shows that the s_z coordinates of the fixed points are given by the real roots of the fourth order polynomial

$$4(g^2+\gamma^2)s_z^4 + 4g\varepsilon s_z^3 + (\varepsilon^2+v^2-g^2-\gamma^2)s_z^2 - g\varepsilon s_z - \varepsilon^2/4 = 0. \quad (47)$$

TABLE I: Classification of fixed points according to the eigenvalues λ_1 and λ_2 of the Jacobi matrix.

$\lambda_1, \lambda_2 \in \mathbb{R}$	$\lambda_1, \lambda_2 < 0$	Stable node (sink)	Index $+1$
	$\lambda_1, \lambda_2 > 0$	Unstable node (source)	Index $+1$
	$\lambda_1 \lambda_2 < 0$	Saddle point	Index -1
$\lambda_{1,2} = \alpha \pm i\beta$	$\alpha < 0$	Stable focus (sink)	Index $+1$
	$\alpha > 0$	Unstable focus (source)	Index $+1$
	$\alpha = 0$	Center	Index $+1$

In the following we will restrict the discussion to the unbiased case $\varepsilon = 0$ where the polynomial (47) becomes biquadratic and the fixed points are easily found analytically. The analysis can in principle be extended to the case $\varepsilon \neq 0$ in a straightforward manner. For $\varepsilon = 0$ the polynomial (47) has the four solutions $s_z = 0, 0, \pm\frac{1}{2}\sqrt{1 - \frac{v^2}{g^2+\gamma^2}}$. The corresponding values of s_x and s_y are then given by (46) and the normalization condition. In summary, this yields the solutions

$$\vec{s}_{c\pm} = \begin{pmatrix} \pm\frac{1}{2}\sqrt{1-\frac{\gamma^2}{v^2}} \\ \frac{\gamma}{2v} \\ 0 \end{pmatrix}, \quad \vec{s}_{f\pm} = \begin{pmatrix} \frac{gv}{2(g^2+\gamma^2)} \\ \frac{\gamma v}{2(g^2+\gamma^2)} \\ \pm\frac{1}{2}\sqrt{1-\frac{v^2}{g^2+\gamma^2}} \end{pmatrix}. \quad (48)$$

Since the components of the Bloch vector are by definition real valued, only the real solutions correspond to actual fixed points. Due to the non-Hermiticity these are not necessarily elliptic fixed points or saddle points, which are the only possibilities in Hamiltonian systems. Rather, as we already observed for the linear non-Hermitian case, the additional gradient flow can lead to a destruction of periodic motion and introduce sinks and sources to the dynamics. In principle it can also lead to the emergence of limit cycles [91, 92] which, however, have not been observed in the study of the present system.

For a flow on a two dimensional surface (as in the case of the Bloch sphere), information on the type of fixed points can be obtained by the surrounding linearized fields (apart from special cases at parameter values for which bifurcations occur, see e.g., [91] and references therein). We will now briefly introduce the classification scheme; further details can be found, e.g., in [93–96].

Suppose we have a system of two first order differential equations which can be written in the form

$$\dot{q}_1 = F_1(q_1, q_2), \quad \dot{q}_2 = F_2(q_1, q_2). \quad (49)$$

The linearization of this system around an arbitrary point is determined by the Jacobi matrix $D_{ij} = \partial F_i/\partial q_j$, $(i, j = 1, 2)$ of the vector field $\vec{F}$ at that point. The eigenvalues $\lambda_{1,2}$ of this matrix at a fixed point of the dynamics, that is, a singular point of the vector field $\vec{F}$, can yield information about the fixed point type. These eigenvalues are either real or form a complex conjugate pair, due to the reality of the matrix. One can distinguish four basic fixed point types (nodes, saddle points, foci and centers) and subclasses according to the values of $\lambda_{1,2}$, which are summarized in Table I.

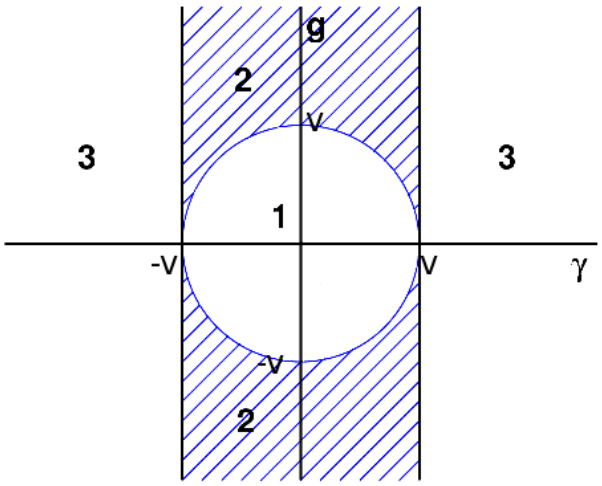

FIG. 7: Parameter regions belonging to different fixed point configurations of the non-Hermitian mean-field dynamics (33).

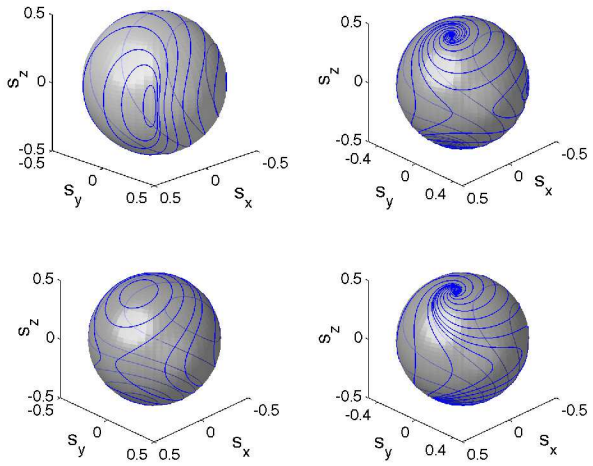

FIG. 8: Mean-field dynamics on the Bloch sphere for $\varepsilon = 0$, $v = 1$ and different values of γ and g. (Left to right and top to bottom: $\gamma = 0.7$, $g = 0.7$; $\gamma = 0.75$, $g = 3$; $\gamma = 0$, $g = 3$; $\gamma = 1.25$, $g = 3$)

The so-called (Poincaré) index, also listed in the table, is a further characteristic quantity of a singular point of a vector field with respect to an oriented surface (see, e.g., [93, 96] for details). It is defined as the number of revolutions of the vector field in traversing an arbitrary curve encircling the (isolated) singular point (and no other singular point). The index of a saddle point is -1, whereas the indices of nodes, foci and centers are all equal to $+1$. The number and type of singular points of a vector field and the possible bifurcation scenarios for a given manifold are restricted by the *index theorem*. It states that the sum of the indices of the singular points of a vector field on a manifold is independent of the choice of the vector field and equals the Euler characteristic χ_E, which is $\chi_E = 2$ in the case of a sphere.

The fixed points of our nonlinear non-Hermitian system (33) can be categorized completely according to the above scheme. In summary, we can distinguish three regions in parameter space, which are sketched in Fig. 7:

1. In region 1, for $\gamma^2 + g^2 \leq v^2$, we have only two fixed points $\vec{s}_{c\pm}$ which are located at the equator. For $g \neq 0$ one of them is a sink, the other one is a source. They degenerate to centers for $g = 0$.

2. In region 2, for $\gamma^2 + g^2 > v^2$ and $|\gamma| < |v|$, there are four coexisting fixed points, namely, a sink and a source, a center, and a saddle point. On the line $\gamma = 0$ the sink and source become centers, corresponding to the Hermitian self-trapping states.

3. In region 3, which is defined by $|\gamma| > |v|$, only the fixed points $\vec{s}_{f\pm}$ exist, namely a sink and a source. For positive γ we have a source on the northern hemisphere and a sink on the southern. In general ($g \neq 0$) they are foci, which become nodes in the linear limit.

At the boundaries of these regions, at the critical parameter values, bifurcations that necessarily respect the index theorem occur.

Figure 8 shows examples of the Bloch dynamics (33) in the three different regions and on the Hermitian line. In the first plot (left on the top) the dynamics is shown for $\gamma = 0.7$ and $g = 0.7$, that is, in region 1. We observe deformed Bloch oscillations surrounding the two centers (index $+1$). If the non-Hermiticity is increased, the centers approach each other along the equator. However, before they meet one of them bifurcates at the critical circle $g^2 + \gamma^2 = v^2$ (and $\gamma \neq 0$) into a saddle (index -1) and two foci (index $+1$), $\vec{s}_{f\pm}$, one stable (a sink) and one unstable (a source).

The second plot (right on the top) in Fig. 8 shows the resulting dynamics above this bifurcation, however still in region 2. Here we observe four fixed points resulting in a mixed dynamics, where besides the periodic motion surrounding the remaining center $\vec{s}_{c\pm}$ there are flows from the source to the sink. The appearance of the two fixed points $\vec{s}_{f\pm}$ can be viewed as a non-Hermitian self-trapping dynamics, which collapses to the Hermitian case in the singular limit $\gamma = 0$. This is depicted in the third plot (left in the lower panel). Here the foci are replaced by centers. The Hermitian self-trapping effect arises as a bifurcation of the center (index $+1$) into a saddle (index -1) and the additional centers (index $+1$) at the critical circle. Thus, the critical value $g_{\rm crit} = \sqrt{v^2 - \gamma^2}$ is decreased for $\gamma \neq 0$ compared to the Hermitian case. In other words, the presence of the non-Hermiticity promotes the self-trapping effect, however, the resulting self-trapping oscillations are damped due to the non-Hermiticity, as we shall discuss later.

In region 2 the dynamics is mainly organized by the stable and unstable manifolds of the saddle point, as shown in Fig. 9 for $g = 3$ and two values of γ. In the Hermitian case, $\gamma = 0$, these manifolds form a single figure-eight curve, a separatrix, encircling the self-trapping regions around the two centres $\vec{s}_{f\pm}$. In addition, there is a third center localized at the equator opposite to the saddle point.

In the non-Hermitian case the two self-trapping centers change into a sink close to the north-pole and a source close

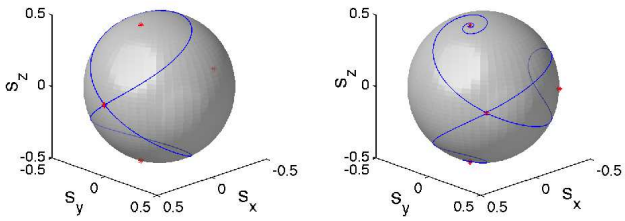

FIG. 9: (Color online) Stable and unstable manifolds of the saddle point $\vec{s}_{c-}$ for $g = 3$ and a Hermitian $\gamma = 0$ (left) and a non-Hermitian case $\gamma = 0.75$ (right). The four fixed points are marked by red dots.

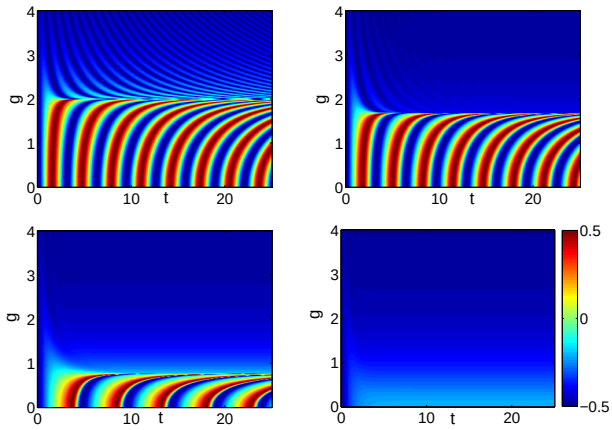

FIG. 10: (Color online) Mean-field dynamics of s_z plotted in false colors in dependence on the nonlinearity g for $v = 1$, $\varepsilon = 0$ where the initial state is the south pole of the Bloch sphere, for different values of the non-Hermiticity (top to bottom and left to right: $\gamma = 0$, $\gamma = 0.2 < v$, $\gamma = 0.75 < v$, and $\gamma = 1.1 > v$).

to the south-pole. The saddle-point and the center at the equator survive and the separatrix through the saddle point transforms into a single curve emanating from the source, passing through the saddle-point, encircling the center, passing again through the saddle and, finally, spiralling into the sink, as shown in the left panel of Fig. 9 for $\gamma = 0.75$. The surface is divided into two regions, an area A_c of oscillatory motion encircling the center, and the rest, the basin of attraction of the sink. With increasing interaction g, the area A_c shrinks into a thin region close to the equator (note that the positions of the center and the saddle point are independent of g). Decreasing the interaction g, the sink and the source approach the saddle-point and meet at the critical value $g_{\rm crit}$. During this process, the area A_c grows until it covers the whole sphere at $g_{\rm crit}$.

For increasing γ, starting from parameter region 2, the saddle point (index -1) and the center (index $+1$) on the equator approach each other along the equator until they meet and annihilate for $\gamma = v$ at $\vec{s} = (0, 1/2, 0)$. For larger values of γ, that is, in region 3 only the source and the sink remain, and the dynamics is fully governed by the flow from the former to the latter, as illustrated in the last plot (right in the lower panel) in Fig. 8. For $g = 0$, the transition occurs directly between region 1 and 3 in a non-generic bifurcation at $\gamma = \pm v$ (the EP), which is depicted in Fig. 3 where the two centers meet and simultaneously change into a sink and a source.

In the Hermitian case, for $g > g_{\rm crit} = v$, we find self-trapping oscillations in the vicinity of the fixed points $\vec{s}_{f\pm}$. For $\gamma \neq 0$ these fixed points change into a sink and a source of the dynamics which results in a damping of the self-trapping oscillations. Figure 10 illustrates this damping effect. Here we plot in false colors the time dependence of s_z, the population imbalance between the two levels, as a function of the nonlinearity g for an initial state at the south pole of the Bloch sphere for four different values of γ. The first plot on the left shows the behavior in the case $\gamma = 0$. We observe two distinct regimes: For $g < g_{\rm sep} = 2$, the starting point, and hence the whole trajectory, is inside the area A_c and the motion $s_z(t)$ shows a large amplitude oscillation extending to the vicinity of the north pole. For $g > g_{\rm sep} = 2$. in the self-trapping region, the motion is confined to the neighborhood of the south pole. At $g_{\rm sep} = 2$ the separatrix passes through the south pole and the motion starting there approaches in infinite time the saddle point along the stable manifold. (Note the increase of the period of oscillation for $g \to g_{\rm sep}$ where the period diverges.) This behavior continues for $\gamma \neq 0$, however with a smaller value of $g_{\rm sep}$. For small nonlinearities the population is completely transferred between the two levels, that is, the Bloch vector oscillates between the south and the north pole and above $g_{\rm sep}$ the oscillation stays closer to the south pole with increasing interaction. As observed in Fig. 8, the self-trapping states are then associated with a sink and a source of the dynamics. Therefore, for a nonvanishing but subcritical non-Hermiticity $0 < \gamma < v$, the system relaxes to a state with excess population in the non-decaying state above a critical value $g_{\rm sep}$ of the interaction. This appears as a damping in the self-trapping oscillations, which is visible in the second and third plot (top right and bottom left) in Fig. 10. A similar observation was reported in [97] where the effect was related to decoherence. For even larger values $\gamma > v$ in region 3, as shown in the right plot in the lower panel in Fig. 10, the oscillatory motion is already destroyed even in the linear case $g = 0$, and the dynamics is dominated by the flow from the sink to the source irrespective of the nonlinearity, that is, the system stays confined to the lower half of the Bloch sphere.

For the non-Hermitian system the normalization n, which can be interpreted as the "survival probability" of the system, is also time dependent. For the non-Hermitian two level system (35) the dynamics are governed by the equation of motion (34), that is, $\dot{n} = -2\gamma(2s_z + 1)n$, which does not explicitly depend on the nonlinearity. Yet, the instantaneous decay rate is determined by the s_z component of the renormalized Bloch vector, whose dynamics are sensitively influenced by the nonlinear term in the Schrödinger equation. This is illustrated in Fig. 11 which shows the half life time as a falsecolor plot, as a function of the initial conditions (p, q) for a weak decay, $\gamma = 0.1$, and different nonlinearities. It is clearly visible that the nonlinearity can stabilize the system significantly for certain initial conditions. (Note the different colorscales.)

To understand this behavior in more detail, we investigate

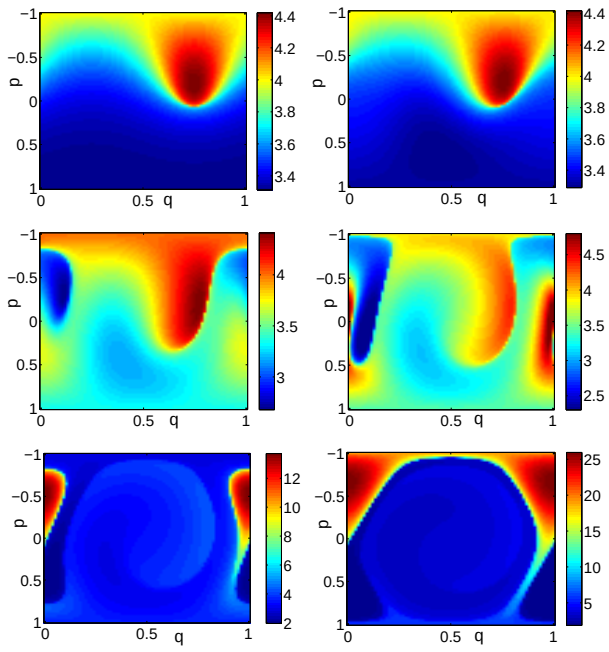

FIG. 11: (Color online) Half life time in dependence on the initial condition for the non-Hermitian mean-field dynamics for $\varepsilon = 0$ for $v = 1$ and $\gamma = 0.1$ and different values of the nonlinearity, (from left to right and top to bottom, $g = 0$, 0.1, 0.5, 1, 1.5, 2).

the full time evolution of the normalization for some examples. In Fig. 12 we show the normalization $n(t) = |\psi_1|^2 + |\psi_2|^2$ of the wave function as a function of time for a small non-Hermiticity $\gamma = 0.1$ and a supercritical nonlinearity $g = 3$ (blue lines), in comparison to the linear evolution for $g = 0$ (black lines). The left plot shows the dynamics for an initial state at the north pole of the Bloch sphere, and the right plot corresponds to a state initially at the south pole. We observe that for an initial condition at the north pole (corresponding to the decaying level) the decrease of the normalization is slightly faster due to the nonlinearity, although from time $t \approx 5$ onward it slows down considerably. In the limit $t \to \infty$ the decrease becomes exponential with a very small decay coefficient. The modulations present in the linear case are much less pronounced here from the very beginning. Despite these differences, the overall decay time characterized, e.g., by the half life time, is not drastically changed here. If we now turn to the right plot and compare the nonlinear decay behavior to the linear one for an initial condition in the south pole of the Bloch sphere (corresponding to the stable level) the induced changes become much more pronounced. In fact, the decay is considerably slowed down by the nonlinearity. For longer times the modulations nearly vanish and the decay becomes approximately exponential with the same decay coefficient as for the initial condition in the north pole.

This behavior can be understood in terms of the Bloch dynamics discussed before. For large nonlinearities the *source* of the Bloch dynamics moves toward the north pole, which is connected with the decaying level and thus a *sink* for the probability. The *sink* of the Bloch dynamics, on the other hand,

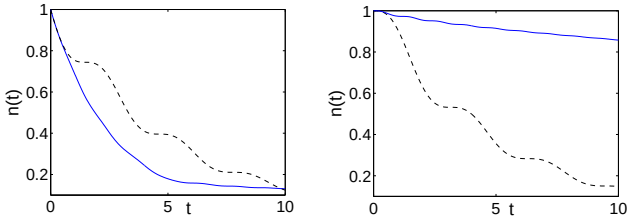

FIG. 12: (Color online) Decay of the mean-field normalization n in dependence on the nonlinearity for a small decay $\gamma = 0.1$. The evolution for a nonlinearity of $g = 3$ (blue solid curves) is compared to the linear case (black dashed curves). The left figure shows the time evolution of $n(t)$ starting in the north pole, the right figure shows the same for an initial state at the south pole.

moves close to the south pole which corresponds to the *stable* level. Thus, if we start the system at the south pole (right plot in Fig. 12), then due to the nonlinearity it stays on the southern hemisphere ($-\frac{1}{2} \leq s_z \leq 0$) and spirals into the sink of the dynamics instead of performing Rabi oscillations extending over all values of s_z. Hence the instantaneous decay rate is smaller than for the linear case and the decay is significantly decelerated. If we start the dynamics at the north pole (left plot in Fig. 12), on the other hand, the Bloch dynamics also move toward the sink close to the south pole, where they remain. However, until the small instantaneous values of the decay coefficient associated with the southern hemisphere of the Bloch sphere become relevant, the normalization already decayed considerably.

Summarizing, the interplay of nonlinearity and non-Hermiticity introduces a qualitatively new behavior to the mean-field dynamics. This is manifested in the different types and numbers of fixed points generated in the renormalized dynamics, and in the resulting sensitivity of the normalization dynamics to the initial conditions.

VI. MANY-PARTICLE MEAN-FIELD CORRESPONDENCE

Let us finally compare the mean-field description with the full many-particle behavior. We begin with a comparison of the spectral behavior. For this purpose we first have to define the eigenenergies of the mean-field system. We will identify them with the values of the Hamiltonian function at the fixed points of the mean-field dynamics. Note that these are different from the generalized eigenvalues of the nonlinear non-Hermitian Schrödinger operator (the chemical potentials) which were investigated in some detail for a closely related model in [47, 81]. Figure 13 shows the real and imaginary parts of the eigenenergies in dependence on γ for two different values of the nonlinearity. For nonvanishing nonlinearity we observe a similar behavior as in the linear case, where the two eigenvalues are purely imaginary until they meet at the critical value $|\gamma| = v$ and turn into a complex conjugate pair. Here, however, the two eigenvalues vanish after their "collision", which is connected to the collision and simultaneous destruc-

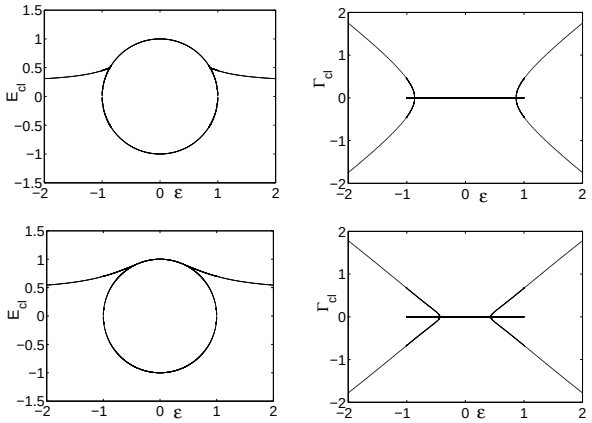

FIG. 13: Real (left) and imaginary (right) part of the mean-field eigenenergies (values of the Hamiltonian function at the fixed points) as a function of γ for $\varepsilon = 0$, $v = 1$ and $g = 0.5$ (top) and $g = 0.9$ (bottom).

tion of the saddle point with the center in the phase space. In particular, the energy values of these two fixed points are identical to the linear case. This is evident from the fact that they are located at the equator of the Bloch sphere, that is, at $s_z = 0$ and thus the nonlinear term (proportional to s_z^2) in the energy vanishes. However, for values of γ above the saddle-center collision, we still have two eigenvalues associated with the sink and the source that result from the bifurcation of one of the original centers at the critical value $|\gamma_{\rm crit}| = \sqrt{v^2 - g^2}$. Their imaginary parts are always nonzero, due to the fact that they are located at values $s_z \neq 0$. Thus, the critical value for the emergence of the sink and the source defines the border of unbroken $\mathcal{PT}$-symmetry for the mean-field system. In agreement with the many-particle results, we conclude that the nonlinearity g shrinks the region of unbroken $\mathcal{PT}$-symmetry.

The observed behavior is evidently the counterpart of the pairwise crossing structure and the unfolding of the EP of higher order in the many-particle spectrum. For a better comparison we show both the many-particle and mean-field eigenenergies in Fig. 14 for the $\mathcal{PT}$-symmetric case as a function of γ for an intermediate interaction strength, $g = 0.9$. We indeed observe that the qualitative phenomenon of the shrinking region of unbroken $\mathcal{PT}$-symmetry is reproduced by the mean-field energies. However, the critical value of γ that defines this border is different for the two descriptions. This is not surprising if we account for two facts: First, we note that the positions of the individual EPs depend on the particle number N, and the large N limit (in which one assumes the mean-field description to be valid) is not reached for $N = 20$ particles, as in the present figure. It is in general an open question in which manner the mean-field limit is approached for non-Hermitian systems. Second, we do not expect an individual feature of the spectrum to have an impact on the classical limit. This is due to the fact that this limit is only defined up to arbitrary orders of $\hbar$ (i.e. $1/N$ in the present case), whereas the exact positions of individual structures, such as exceptional points, is dependent on these additional terms. Therefore, usually isolated degeneracies do not have counterparts in the associated classical limit. Only if there is an accumulation of such points one expects a direct correspondence. Nonetheless, in the present case the $\mathcal{PT}$-symmetry itself is mirrored in the classical system and thus we expect the breaking of this symmetry to be present as well. This is in agreement with the observed behavior for which the breaking of the symmetry takes place both in the mean-field and the many-particle system, and the influence of the interaction shrinks the region of unbroken $\mathcal{PT}$ symmetry in both cases.

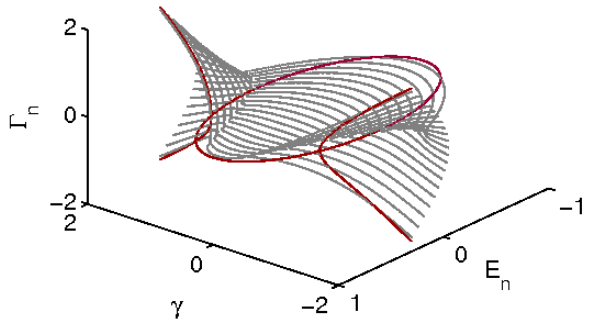

FIG. 14: (Color online) Many-particle (gray) and mean-field (dark red) energies for the $\mathcal{PT}$-symmetric system ($\varepsilon = 0$) for $N = 20$ particles as functions of γ, for $v = 1$ and $g = 0.9$.

To get some insights into the correspondence of the mean-field and many-particle dynamics, we show several examples in Figs. 15 and 16. The figures on the top show the dynamics of the mean-field and the many-particle Bloch vector for a state initially located at the north pole of the Bloch sphere. For a better comparison we depict the dynamics of the corresponding z-component, that is, the relative population imbalance of the two modes, in the plots in the middle. The resulting time dependence of the overall probability is shown in the lower plots. Here we have to compare the mean-field probability $n(t)$, given by the normalization of the single particle wave function, to the normalization of the many-particle wave function in the following way:

$$n(t) = |\psi_1(t)|^2 + |\psi_2|^2 \longleftrightarrow \sqrt[N]{\langle\Psi(t)|\Psi(t)\rangle}, \qquad (50)$$

thus accounting for different values of the particle number N.

Let us first focus on Fig. 15 where we show the dynamics for $N = 20$ particles. The left column shows an example where both the interaction strength and the non-Hermiticity are small ($g = 0.5$ and $\gamma = 0.1$). The classical mean-field dynamics shows the typical deformed Rabi oscillations. In the many-particle system we observe the familiar breakdown behavior. Numerical results for a longer propagation suggest that the revival phenomena are strongly suppressed by the non-Hermiticity. The right column shows the dynamics for a stronger interaction and a stronger decay ($g = 2$

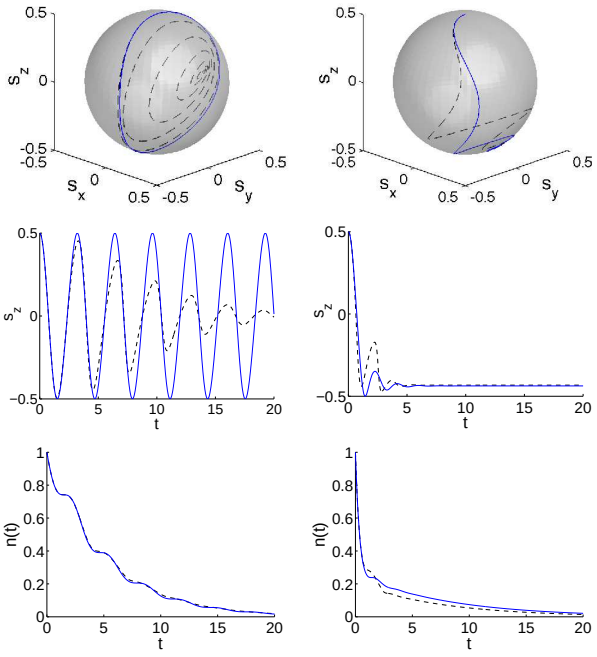

FIG. 15: (Color online) Many-particle (dashed black lines) for $N = 20$ particles and mean-field (solid blue lines) dynamics for an initial state in mode 1, that is, the north pole of the Bloch sphere with $v = 1$, $\varepsilon = 0$ and $g = 0.5$, $\gamma = 0.1$ (left plots), $g = 2$, $\gamma = 0.5$ (right plots). The upper plots show the dynamics of the angular momentum expectation values and the mean-field Bloch vector, respectively. The middle panels show the corresponding z-component and the lower plots the evolution of the overall probability $n(t)$.

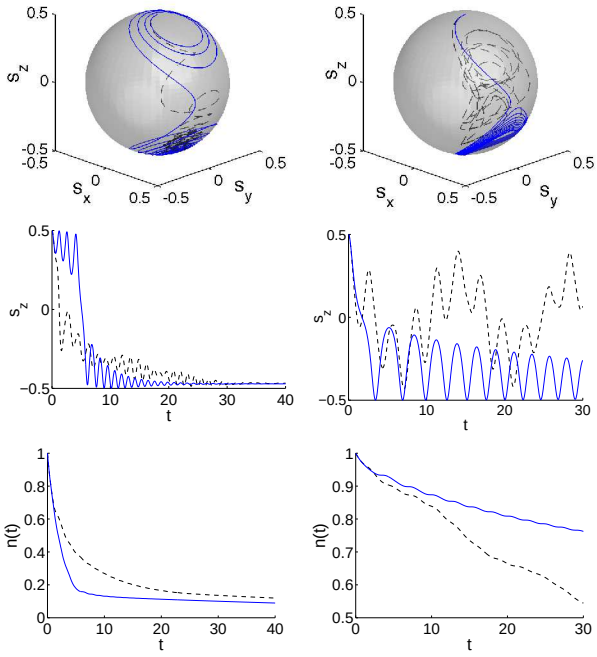

FIG. 16: (Color online) Many-particle (dashed black lines) and mean-field (solid blue lines) dynamics for different parameters and an initial state in mode 1, that is, the north pole of the Bloch sphere. As in Fig. 15 but for the parameters $v = 1$, $\varepsilon = 0$ and $g = 3$, $\gamma = 0.1$, and $N = 20$ particles (left plots) and $g = 2$, $\gamma = 0.01$, and $N = 5$ particles (right plots).

and $\gamma = 0.5$), i.e. in the mean-field self-trapping region. The mean-field trajectory, commenced from the north pole, approaches the fixed point located at $s_z = -0.433$. The full many-particle system shows a very similar behavior. For both examples the many-particle survival probability, depicted in the lower panel, is also reproduced by the mean-field approximation. In the regime of strong interaction, we can also observe more complicated behavior, including phenomena related to a many-particle tunneling from one self-trapping state to the other. This is illustrated in Fig. 16 where we plot the dynamics for large values of the interaction strength and comparatively small values of γ for an initial state at the north pole. The left column shows an example with $N = 20$ particles for the parameters $g = 3$ and $\gamma = 0.1$. One clearly observes a tunneling of the many-particle dynamics between the mean-field stationary states. However, due to the fact that the stationary state on the south pole of the sphere is the sink of the mean-field dynamics, the latter approaches the southern fixed point as well. The right column shows a similar example with only $N = 5$ particles for a slightly smaller interaction strength $g = 2$ and a very small decay $\gamma = 0.01$, to make the tunneling process apparent. This superimposed many-particle effect induces a clear mismatch into the correspondence of the survival-probability evolution, which is illustrated in the lower panels.

The approach to the mean-field limit with increasing particle number can be illustrated by comparison of the half life time of the normalization as a function of the initial conditions for different particle numbers. In Fig. 17 we show the half life time as a function of the initial position on the Bloch sphere for $\gamma = 0.1$ and $g = 1$ and different particle numbers. The corresponding mean-field behavior is depicted in the right plot in the middle row of Fig. 11 with the same colorscale. It can be nicely seen how the mean-field features become more pronounced with increasing particle number.

The presented results give a first impression on the intricate correspondence of the full many-particle description and the mean-field approximation for this non-Hermitian system. Further investigations of this correspondence and in particular the manner in which the mean-field limit is approached are promising topics for future investigations.

VII. SUMMARY AND OUTLOOK

We have studied the dynamics of a non-Hermitian two-mode Bose-Hubbard system and a related $\mathcal{PT}$-symmetric model. We have derived a non-Hermitian mean-field approximation, which can be expressed in a generalized canonical form, including a metric gradient flow [22], and demonstrated the close correspondence of the damped (pseudo)classical motion in this mean-field description and the quantum many-

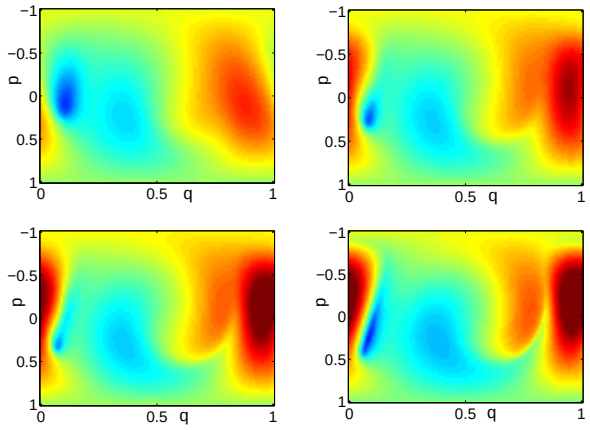

FIG. 17: Half life time of the rescaled normalization $\sqrt[N]{\langle\Psi(t)|\Psi(t)\rangle}$ of the many-particle wave function for $\varepsilon = 0$ for $v = 1$, $\gamma = 0.1$, $g = 1/N$ and different particle numbers (from left to right and top to bottom: $N = 5$, 10, 15, 30).

particle evolution. In particular, we have analyzed the fixed point structure of the mean-field dynamics and its bifurcation arising when the system parameters are varied. This results in a rich variety of phenomena in the many-particle dynamics, as for instance breakdown and revival, and tunneling, which can be interpreted easily in terms of the underlying mean-field structure.

In conclusion, the combined presence of interaction and non-Hermiticity introduces a variety of interesting phenomena into the correspondence between the many-particle dynamics and the mean-field description. The understanding of general quantum classical correspondence for non-Hermitian systems will ultimately require the development of new taylor-made methods, such as the Husimi-Schur phase space representation [40] that was recently suggested in the context of open quantum maps. The simple model presented here provides an ideal testing ground for new methods for non-Hermitian systems. Future investigation and categorization of its behavior are thus a promising starting point for the formulation of a general framework for quantum classical correspondence in the presence of non-Hermiticity.

Acknowledgments

Support from the Deutsche Forschungsgemeinschaft via the Graduiertenkolleg "Nichtlineare Optik und Ultrakurzzeitphysik" is gratefully acknowledged. We thank Dorje Brody for helpful discussions and comments.

Appendix A: The generalized canonical equations in terms of the coordinates φ_j

The nonlinear complex Schrödinger equation (37) can also be expressed in terms of a generalized canonical equation of motion, in the complex form

$$\mathrm{i}\begin{pmatrix}\dot{\varphi}\\ \dot{\varphi}^*\end{pmatrix} = \Omega^{-1}\vec{\nabla}H - \mathrm{i}G^{-1}\vec{\nabla}\Gamma, \tag{A1}$$

where we have to pick two canonical conjugate variables φ and φ^* from the four variables $\varphi_1, \varphi_1^*, \varphi_2, \varphi_2^*$. Although the dynamics is apparently governed by all four variables the normalization is fixed and the dynamics is independent of the global phase. Therefore, we have only two independent variables which we can choose out of the original four. It is convenient to choose φ_1 and φ_1^* rather than φ_1 and φ_2. They are connected to the coordinates p, q via

$$\varphi_1 = \sqrt{\frac{p+1}{2}}\mathrm{e}^{-2\mathrm{i}q}, \quad \varphi_1^* = \sqrt{\frac{p+1}{2}}\mathrm{e}^{2\mathrm{i}q}. \tag{A2}$$

The equation of motion for the other variables are then implicitly provided. With the choice φ_1 and φ_1^* for the independent variables we automatically demanded φ_2 to be real and fulfill the normalization condition $\varphi_2 = \varphi_2^* = \sqrt{1-\varphi_1^*\varphi_1}$. The symplectic matrix is the familiar one and for the inverse of the Kähler metric we find:

$$\left(G^{(\varphi_1,\varphi_1^*)}\right)^{-1} = \begin{pmatrix} \frac{\varphi_1^2(|\varphi_1|^2-2)}{2(1-|\varphi_1|^2)} & \frac{2-2|\varphi_1|^2+|\varphi_1|^4}{2(1-|\varphi_1|^2)} \\ \frac{2-2|\varphi_1|^2+|\varphi_1|^4}{2(1-|\varphi_1|^2)} & \frac{\varphi_1^{*2}(|\varphi_1|^2-2)}{2(1-|\varphi_1|^2)} \end{pmatrix}. \tag{A3}$$

The equations of motion for φ_1 and φ_1^* can then be found from (A1), where H and Γ are given by the real and imaginary parts of the Hamiltonian function for the non-Hermitian and nonlinear two-level system expressed in terms of φ_1 and φ_1^*:

$$\mathcal{H} = (\varepsilon - \mathrm{i}\gamma)(\varphi_1^*\varphi_1 - 1) + v\sqrt{1-\varphi_1^*\varphi_1}(\varphi_1^* + \varphi_1) + \frac{g}{2}(\varphi_1^*\varphi_1 - 1)^2. \tag{A4}$$

The equation of motion for φ_2 can then be deduced from the dynamics of φ_1 via

$$\dot{\varphi}_2 = -\frac{\dot{\varphi}_1\varphi_1^* + \varphi_1\dot{\varphi}_1^*}{2\sqrt{1-\varphi_1\varphi_1^*}}. \tag{A5}$$

The dynamics thus obtained is equivalent to the non-Hermitian (nonlinear) Schrödinger equation (37) up to a global phase.

[1] L. Pitaevskii and S. Stringari, *Bose-Einstein Condensation*, Oxford University Press, Oxford, 2003
[2] S. Weinberg, Ann. Phys. (N.Y.) **194** (1989) 336
[3] R. Franzosi, and V. Penna, and R. Zecchina, Int. J. Mod. Phys. B **14** (2000) 943
[4] S. Mossmann and C. Jung, Phys. Rev. A **74** (2006) 033601
[5] A. R. Kolovsky, Phys. Rev. Lett. **99** (2007) 020401
[6] F. Trimborn, and D. Witthaut, and H. J. Korsch, Phys. Rev. A **77** (2008) 043631
[7] F. Trimborn, and D. Witthaut, and H. J. Korsch, Phys. Rev. A

79 (2009) 013608
[8] M. Hiller, T. Kottos, and T. Geisel, Phys. Rev. A **79** (2009) 023621
[9] G. J. Milburn, J. Corney, E. M. Wright, and D. F. Walls, Phys. Rev. A **55** (1997) 4318
[10] M. J. Steel, and M. J. Collett, Phys. Rev. A **57** (1998) 2920
[11] R. Franzosi, and V. Penna, Phys. Rev. A **63** (2001) 043609
[12] Y. Wu, and X. Yang, Phys. Rev. A **68** (2003) 013608
[13] K. W. Mahmud, H. Perry, and W. P. Reinhardt, Phys. Rev. A **71** (2005) 023615
[14] B. Wu and J. Liu, Phys. Rev. Lett. **96** (2006) 020405
[15] E. M. Graefe and H. J. Korsch, Phys. Rev. A **76** (2007) 032116
[16] E. Boukobza, M. Chuchem, D. Cohen, and A. Vardi, Phys. Rev. Lett. **102** (2009) 180403
[17] G. Gamow, Z. Phys. A **51** (1928) 204
[18] G. Dattoli, A. Torre, and R. Mignani, Phys. Rev. A **42** (1990) 1467
[19] J. Okolowicz, M. Ploszajczak, and I. Rotter, Phys. Rep. **374** (2003) 271
[20] N. Moiseyev, Phys. Rep. **302** (1998) 211
[21] M. V. Berry, Czech. J. Phys. **54** (2004) 1039
[22] E. M. Graefe, M. Höning, and H. J. Korsch, J. Phys. A **43** (2010) 075306
[23] C. Mahaux and H. A. Weidenmüller, *Shell Model Approach to Nuclear Reactions*, North Holland Pub. Comp., Amsterdam, 1969
[24] C. M. Bender and S. Boettcher, Phys. Rev. Lett. **80** (1998) 5243
[25] C. M. Bender, D. C. Brody, and H. F. Jones, Phys. Rev. Lett. **89** (2002) 270401
[26] J. Phys. A **39**(32), (2006), *Special issue dedicated to the physics of non-Hermitian operators*.
[27] R. El-Ganainy, K. G. Makris, D. N. Christodoulides, and Z. H. Musslimani, Opt. Lett. **32** (2007) 2632
[28] Z. H. Musslimani, K. G. Makris, R. El-Ganainy, and D. N. Christodoulides, Phys. Rev. Lett. **100** (2008) 030402
[29] S. Klaiman, U. Günther, and N. Moiseyev, Phys. Rev. Lett. **101** (2008) 080402
[30] S. Longhi, Phys. Rev. Lett. **103** (2009) 123601
[31] O. Bendix, R. Fleischmann, T. Kottos, and B. Shapiro, Phys. Rev. Lett. **103** (2009) 030402
[32] C. T. West, T. Kottos, and T. Prosen, Phys. Rev. Lett. **104** (2010) 054102
[33] H. Schomerus, Phys. Rev. Lett. **104** (2010) 233601
[34] A. Guo, G. J. Salamo, D. Duchesne, R. Morandotti, M. Volatier-Ravat, V. Aimez, G. A. Siviloglou, and D. N. Christodoulides, Phys. Rev. Lett. **103** (2009) 093902
[35] C. E. Rüter, K. G. Makris, R. El-Ganainy, D. N. Christodoulides, M. Segev, and D. Kip, Nature Physics **6** (2010) 192
[36] H. Schomerus, and P. Jacquod, J. Phys. A **38** (2005) 10663
[37] C. M. Bender, D. W. Hook, P. N. Meisinger, and Q. Wang, Phys. Rev. Lett. **104** (2010) 061601
[38] H. F. Jones and E. S. Moreira Jr, J. Phys. A **43** (2010) 055307
[39] J. P. Keating, M. Novaes, S. D. Prado, and M. Sieber, Phys. Rev. Lett. **97** (2006) 150406
[40] M. Kopp and H. Schomerus, Phys. Rev. E **81** (2010) 026208
[41] N. Moiseyev and L. S. Cederbaum, Phys. Rev. A **72** (2005) 033605
[42] N. Moiseyev, L. D. Carr, B. A. Malomed, and Y. B. Band, J. Phys. B **37** (2004) L193
[43] P. Schlagheck and T. Paul, Phys. Rev. A **73** (2006) 023619
[44] T. Paul, M. Hartung, K. Richter, and P. Schlagheck, Phys. Rev. A **76** (2007) 063605
[45] K. Rapedius and H. J. Korsch, Phys. Rev. A **77** (2008) 063610
[46] K. Rapedius and H. J. Korsch, J. Phys. B **42** (2009) 044005
[47] E. M. Graefe and H. J. Korsch, Czech. J. Phys. **56** (2006) 1007
[48] R. Livi, R. Franzosi, and G.-L. Oppo, Phys. Rev. Lett. **97** (2006) 060401
[49] R. Franzosi, R. Livi, and G.-L. Oppo, J. Phys. B **40** (2007) 1195
[50] G. S. Ng, H. Hennig, R. Fleischmann, T. Kottos, and T. Geisel, New Journal of Physics **11** (2009) 073045
[51] E. M. Graefe, H. J. Korsch, and A. E. Niederle, Phys. Rev. Lett. **101** (2008) 150408
[52] M. Hiller, T. Kottos, and A. Ossipov, Phys. Rev. A **73** (2006) 063625
[53] E. M. Graefe, U. Günther, H. J. Korsch, and A. E. Niederle, J. Phys. A **41** (2008) 255206
[54] A. N. Kaufman, Phys. Lett. A **100** (1984) 419
[55] P. J. Morrison, Physica D **18** (1986) 410
[56] A. M. Bloch, R. W. Brockett, and T. S. Ratiu, Com. Math. Phys. **147** (1992) 57
[57] A. M. Bloch, P. S. Krishnaprasad, J. E. Marsden, and T. S. Ratiu, Comm. Math. Phys. **175** (1996) 1
[58] D. D. Holm, V. Putkaradze, and C. Tronci, C. R. Math. Acad. Sci. Paris **345** (2007) 297
[59] A. Mondragón and E. Hernández, J. Phys. A **26** (1993) 5595
[60] W. D. Heiss, Phys. Rev. E **61** (2000) 929
[61] F. Keck, H. J. Korsch, and S. Mossmann, J. Phys. A **36** (2003) 2125
[62] U. Günther, F. Stefan, I. Rotter, and B. Samsonov, J. Phys. A **40** (2007) 8815
[63] M. V. Berry and M. Wilkinson, Proc. R. Soc. Lond A **392** (1984) 15
[64] T. Kato, *Perturbation theory for linear operators*, Springer Verlag, Berlin, 1966
[65] C. Dembowski, H.–D. Gräf, H. L. Harney, A. Heine, W. D. Heiss, H. Rehfeld and A. Richter, Phys. Rev. Lett. **86** (2001) 787
[66] H. Cartarius, J. Main, and G. Wunner, Phys. Rev. Lett. **99** (2007) 173003
[67] J. Wiersig, S. W. Kim, and M. Hentschel, Phys. Rev. A **78** (2008) 053809
[68] P. E. G. Assis and A. Fring, J. Phys. A **42** (2009) 015203
[69] M. Holthaus and S. Stenholm, Eur. Phys. J. B **20** (2001) 451
[70] L. G. Yaffe, Rev. Mod. Phys. **54** (1982) 407
[71] W.-M. Zhang, D. H. Feng, and R. Gilmore, Rev. Mod. Phys. **62** (1990) 867
[72] P. Buonsante, and V. Penna, J. Phys. A **41** (2008) 17530
[73] A. M. Perelomov, *Generalized Coherent States and Their Applications*, Springer, Berlin, 1986
[74] D. C. Brody, A. C. T. Gustavsson, and L. P. Hughston, J. Phys. A **41** (2008) 475301
[75] F. Trimborn, D. Witthaut, and S. Wimberger, J. Phys. B **41** (2008) 171001
[76] D. Witthaut, F. Trimborn, and S. Wimberger, Phys. Rev. Lett. **101** (2008) 200402
[77] S. Morrison and A. S. Parkins, Phys. Rev. A **77** (2008) 043810
[78] S. Morrison and A. S. Parkins, Phys. Rev. Lett. **100** (2008) 040403
[79] S. Morrison and A. S. Parkins, J. Phys. B **41** (2008) 195502
[80] H. Schanz, I. Barvik, and B. Esser, Phys. Rev. B **55** (1997) 11308
[81] D. Witthaut, E. M. Graefe, S. Wimberger, and H. J. Korsch, Phys. Rev. A **75** (2007) 013617
[82] K. G. Makris, R. El-Ganainy, D. N. Christodoulides, and Z. H. Musslimani, Phys. Rev. Lett. **100** (2008) 103904
[83] V. I. Arnold, *Mathematical Methods of Classical Mechanics*, Springer, New York, 1978

[84] D. C. Brody and H. L. P. Hughston, J. Geom. Phys. **38** (2001) 19
[85] V. S. Shchesnovich, and V. V. Konotop, Phys. Rev. A **81** (2010) 053611
[86] J. Llibre and C. Pessoa, Extracta Math. **21** (2006) 167
[87] J. Llibre and C. Pessoa, Rend. Circ. Mat. Palermo (2) **55** (2006) 63
[88] J. Llibre and C. Pessoa, Rend. Circ. Mat. Palermo (2) **58** (2009) 361
[89] C. Gutierrez and J. Llibre, Extracta Math. **17** (2002) 289
[90] B. Wu and Q. Niu, Phys. Rev. A **61** (2000) 023402
[91] H. J. Korsch, H.-J. Jodl, and T. Hartmann, *Chaos – A Program Collection for the PC*, Springer, 2008
[92] J. Guckenheimer and P. Holmes, *Nonlinear Oscillations, Dynamical Systems, and Bifurcations of Vector Fields*, Springer, New York, 1983
[93] V. I. Arnold, *Ordinary differential equations*, Springer, Berlin,New York, 2006
[94] F. Dumortier, J. Llibre, and J. C. Artés, *Qualitative theory of planar differential systems*, Springer, Berlin, 2006
[95] A. P. Seyranian and A. A. Mailybaev, *Multiparameter stability theory with mechanical applications*, World Scientific, Singapore, 2003
[96] V. I. Arnold, *Geomtetrical Methods in the Theory of Ordinary Differential Equations*, Springer, New York, 1988
[97] W. Wang, L. B. Fu, and X. X. Yi, Phys. Rev. A **75** (2007) 045601